Thesis for a Master's Degree

Performance Improvement on Path following and Autopilot of ship using Unknown Disturbance Estimation and Separation Principle

Advisor: Prof. Jong-Hwa Kim

February 2018

Department of Convergence Study on the Ocean Science and Technology
Ocean Science and Technology School
Korea Maritime and Ocean University

Min-Kyu Kim

Approved by the committee of the Ocean Science and Technology School of Korea Maritime and Ocean University in partial fulfillment of the requirements for the degree of Mater of science Engineering

Dissertation Committee :

Prof. Gang-Gyoo Jin _____

Prof. Seok-Je Cho _____

Prof. Jong-Hwa Kim _____

December 27, 2017

Department of Convergence Study on the Ocean Science and Technology
Ocean Science and Technology School
Korea Maritime and Ocean University

Contents

List of Figures

List of Tables

미지의 외란 추정과 분리원리를 이용한 선박의 항로 추종 및 오토파일럿 성능 개선

김 민 규

한국해양대학교 해양과학기술전문대학원
해양과학기술융합학과

요약

선박 운항에 있어서 가장 중요한 사항은 항해중 발생할 수 있는 침몰 또는 충돌로부터 선박의 안정성을 확보하고 환경적 외란(파도, 바람, 해류등)이 인가된 경우에도 정해진 항로를 정확하게 추종하는 것이다. 정확한 항로 추종은 선박의 추진 에너지의 손실을 최소화 하며 목적지까지 최단시간에 도달하도록 한다.

현재 선박에 많이 사용되고 있는 회두각 유지 제어기로서 PD형 제어기는 변침각이 큰 경우 오버슈트를 발생시켜 항로에서 벗어나는 원인으로 작용하고 또한 잦은 조타와 변침각의 변화가 거칠게 일어나 선박의 에너지 손실을 증가시킨다. 이와 같은 단점을 보완하기 위해서 속도형 퍼지 PID 오토파일럿 시스템을 적용하였다. 또한 실제의 오토파일럿 시스템은 잡음의 영향을 받아 성능이 저하되는데 이를 보완하기 위해서 Kalman 필터를 이용한 분리원리를 적용하여 성능을 개선시켰다.

그러나 실제 선박이 운항함에 있어서는 환경적 외란으로 인해 발생하는 힘과 모멘트가 선박에 인가되어 선박은 정해진 항로를 정확하게 추종할 수 없고 항로에서 이탈하게 된다. 이를 보완하기 위해서 Kalman 필터의 이노베이션 특성을 이용하여 미지의 외란의 존재가 판단되었으면 이를 퍼지 외란 추정기에서 힘과 모멘트를 추정하고, 이를 실제 선박을 제어하는 추력과 타각으로 변환하여 선박이 정해진 항로를 크게 벗어나지 않고 추종하도록 하였다.

키워드: Kalman 필터; 속도형 퍼지 PID 오토파일럿 시스템; 퍼지 외란 추정기; Kalman 필터를 이용한 분리원리.

Performance Improvement on Path following and Autopilot of ship using Unknown Disturbance Estimation and Separation Principle

Min-Kyu Kim

Department of Convergence Study on the Ocean Science and Technology

Graduate School of Korea Maritime and Ocean University

Abstract

The most important thing in ship operation is to assure the stability of ship from sinking or collision that may occur during navigation, and is for ship to follow the designated route accurately even when environmental disturbances (current, wave, and wind) are applied. Accurate path following minimizes the loss of propulsion energy of the ship and allows it to reach the destination in the shortest time.

The PD type autopilot system, which is widely used in ships, has an overshoot when the rudder angle is large and acts as a cause that the position of ship deviates from the route. And also, the change of the rudder angle becomes rough so that energy loss of the ship is increased. To overcome these disadvantages, a velocity type fuzzy PID autopilot system is applied. However autopilot system is affected by noise, so that the performance of the autopilot system is degraded. To compensate for this, the separation principle using the Kalman filter is applied to improve the performance.

By the way, in actual navigation of the ship, if the forces and moments generated by environmental disturbances are applied to the ship, the ship can not follow the designated route correctly and deviates from the route. In order to compensate for this, if the existence of unknown disturbances are judged by using the innovation characteristic of the Kalman filer, the forces and moments are estimated in the fuzzy disturbance estimator and converted into the thrust and rudder angle controlling the ship.

KEY WORDS: Kalman Filter; Velocity Type Fuzzy PID Autopilot System; Fuzzy Disturbance Estimator; Separation Principle using Kalman Filter.

Chapter 1 Introduction

1.1 Background of a research

Accurate path-following is essential to reach the destination in the shortest time and to minimize the loss of propulsion energy and is essential for economic navigation. And it meets the purpose of ship automation. In order to automate the ship navigation, first, a route decision algorithm that can determine the route must be developed, second, a guidance system that allows the ship to follow the determined route must be developed [9], and finally, an autopilot system that controls the ship according to guidance of the guidance system must be developed [1][2].

In order to accurately control the ship according to the guidance system, an autopilot system is required, which can alter course fast and accurately, can be robust to nonlinearity, and that can not exhibit overshoot when heading angle change is large. The PD type autopilot has been being applied to most ships because its performance and stability were verified. However, due to the limitations as linear controller, it has performance limitation in case nonlinearity is strong. In addition, it exhibits a steady state error because integral operation is not included. Consequently PD controller has limitation in

path following besides heading angle keeping. Therefore, it is necessary to study the velocity type fuzzy PID autopilot system which can solve this limitation [6][7].

Such a fuzzy PID autopilot system has excellent performance if it is not affected by noise. However, most real autopilot systems are affected by measurement noise when receiving measurements from GPS and gyro compass. Therefore, the autopilot system using the fuzzy PID control technique can not have good control performance because of the malfunction of D control operation due to noise. In order to control the linear time-invariant system including the noise, the state of the system should be estimated within a reliable estimation error range. Kalman filter is widely used for the estimation of the state of such a system.

Even if the fuzzy PID autopilot system with excellent performance is used, if unknown disturbances such as current, wind and wave are applied outside of the ship, the ship can not follow the designated route and deviates the route. Noise and unknown disturbances degrade the control performance of the autopilot system. To solve this problem, this paper introduces Kalman filter based state estimation algorithm which combines separation principle and fuzzy disturbance estimation technique. First, the real state of the autopilot system based on the Kalman filter is estimated and the estimated output is feedback to the input of the autopilot system to reduce the influence of noise. Second, the effect of unknown disturbances is compensated by designing the fuzzy disturbance estimator using the innovation characteristics of the Kalman filter.

In order to verify the performance of the proposed Kalman filter based fuzzy PID type autopilot system, the performance of the ship modeled as a linear time invariant discrete stochastic system is addressed.

1.2 Organization of thesis

In chapter 2 of this paper the ship modeling method is described and simulations are performed assuming that the PD type autopilot system is not subjected to noise and unknown disturbances.

In order to improve the disadvantages of the PD type autopilot system, which is used as the heading angle keeping controller, In chapter 3, velocity type fuzzy PID controller is constructed and simulations are performed to verify the control performance of fuzzy PID autopilot system

Chapter 4 of this paper explains how to model the current, wind, and wave that acts as environmental disturbances to create an environment similar to the actual navigation conditions of a ship. And, based on the velocity type fuzzy PID controller autopilot system, simulations are performed when environmental disturbances are applied, in order to examine how the environmental disturbances affects the ship navigation.

In order to improve the control performance of the linear time-invariant discrete stochastic system of a ship affected by noise, Chapter 5 introduces the separation principle and constructs a control algorithm of velocity type fuzzy PID autopilot system based on Kalman filter. And then the control performance through simulations is discussed.

In Chapter 6, fuzzy disturbance estimation algorithm that estimates an unknown disturbances using innovation process of the Kalman filter when an unknown disturbances is applied outside of the ship is suggested. And then the fuzzy disturbance estimator is combined with velocity type fuzzy PID controller autopilot system based on Kalman filter. To verify the performance of the proposed algorithm, the control performance through simulations is investigated.

Since the elements that controls the actual ship is the thrust propeller and rudder angle, in chapter 7, the estimated disturbances are transformed into thrusts and steering angle of ship. Simulations are executed whether the thrusts and the steering angle added to the controller output reduce the influence of unknown disturbances or not. By analyzing simulation results, the effectiveness of the suggested control algorithm is verified.

In Chapter 8, this paper is evaluated and the conclusion is addressed.

Chapter 2 Modeling of ship

In chapter 2, the variables used to express ship motion are defined and the 3 DOF nonlinear and linear ship equations of motion based on 6 DOF nonlinear ship equations of motion taking into the ship's rigid and hydrodynamic characteristics are derived [3].

2.1 Body-fixed coordinate frame and definition of notation used for ship motion

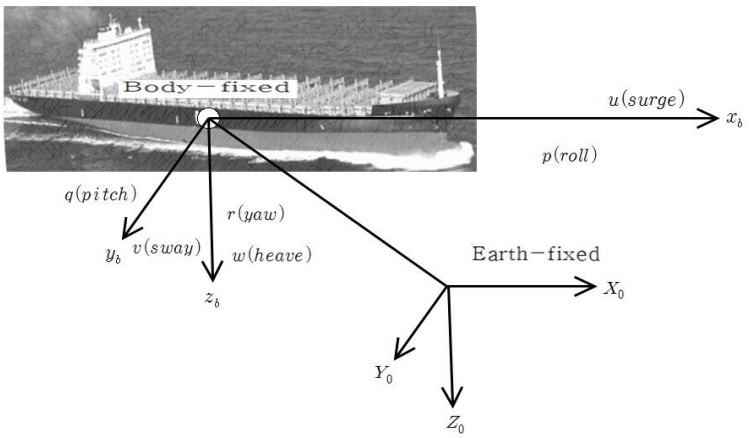

Fig. 2.1 Motion variables for marine vessel

Figure 2.1 and Table 2.1 show the variables for a ship motion and the notation of SNAME for ship. The x_b, y_b and z_b coordinate system is used to describe the main variables of ship motion in the body-fixed coordinate system where origin is fixed to the center of gravity of the ship. X, Y, and Z represent the forces in the x_b, y_b, and z_b direction, K, M, and N represent the moments about the x_b, y_b, and z_b axis. u, v, and w represent linear velocity in the x_b, y_b, and z_b direction, p, q, and r represent the angular velocities about the x_b, y_b, and z_b axis. x, y, and z represent absolute position of a ship with reference to earth-fixed coordinate system. ϕ, θ and ψ represent Euler angles about X_o, Y_o, and Z_o axis.

Table 2.1 The notation of SNAME for marine vessel

DOF	forces and moments	linear and angular velocity	position and Euler angles
1	X	u	x
2	Y	v	y
3	N	w	z
4	K	p	ϕ
5	M	q	θ
6	N	r	ψ

2.2 6 DOF nonlinear ship equation of motion

The motion of ship can be divided into a rigid body dynamic equation and a hydrodynamic equation. The vector model of the 6 DOF nonlinear model is shown in Equation (2.1) [13].

$$M\dot{\nu} + C(\nu)\nu + D(\nu)\nu + g(\eta) = \tau + \tau_{disturbance} \tag{2.1}$$

In Equation (2.1), M is the inertia matrix, $C(\nu)$ the Coriolis matrix, $D(\nu)$ the damping matrix, $g(\eta)$ the restoring force vector related to the force and moment of gravity and buoyancy, τ the force and moment including the thrust and steering force required for the ship to operate, and $\tau_{disturbance}$ is $\tau_{current}+\tau_{wave}+\tau_{wind}$ which means the sum of the forces and moments due to current, wave, and wind acting as disturbances. In this paper, in order to create a realistic environment, three representative disturbances current, wind, and wave are selected and applied.

2.2.1 Rigid-body ship equation of motion

(1) SNAME Notation

The variables of the rigid-body ship equation of motion are defined as follows according to the SNAME notation.

$f_0 = [X, Y, Z]^T$	force
$m_0 = [K, M, N]^T$	moment
$\nu_1 = [u, v, r]^T$	linear velocity
$\nu_2 = [p, q, r]^T$	angular velocity
$r_G = [x_G, y_G, z_G]^T$	center of gravity

Using the Newtonian mechanics and Euler's theorem, the 6 DOF rigid-body ship equations of motion can be express as Equation (2.2) ~ (2.7).

$$m[\dot{u}-vr+wq-x_G(q^2+r^2)+y_G(pq-\dot{r})+z_G(pr+\dot{q})] = X \quad (2.2)$$

$$m[\dot{v}-wp+ur+x_G(qp+\dot{r})-y_G(r^2+p^2)+z_G(qr-\dot{p})] = Y \quad (2.3)$$

$$m[\dot{w}-wq+vp+x_G(rp-\dot{q})+y_G(rq+\dot{p})-z_G(p^2+q^2)] = N \quad (2.4)$$

$$I_x\dot{p}+(I_z-I_y)qr-(\dot{r}+pq)I_{xz}+(r^2-q^2)I_{yz}+(pr-\dot{q})I_{xy} \\ +m[y_G(\dot{w}-uq+vp)-z_G(\dot{v}-wp+ur)]=K \tag{2.5}$$

$$I_y\dot{q}+(I_x-I_z)rp-(\dot{p}+qr)I_{xz}+(p^2-r^2)I_{zx}+(qp-\dot{r})I_{yz} \\ +m[z_G(\dot{u}-vr+wq)-x_G(\dot{w}-uq+vp)]=M \tag{2.6}$$

$$I_z\dot{r}+(I_y-I_x)pq-(\dot{q}+rp)I_{yz}+(q^2-p^2)I_{xy}+(rq-\dot{p})I_{zx} \\ +m[x_G(\dot{v}-wp+ur)-y_G(\dot{u}-vr+wq)]=N \tag{2.7}$$

Here, Equation (2.2) ~ (2.4) represent the ship's translational motion, while Equation (2.5) ~ (2.7) represent the ship's rotational motion. I_x, I_y, I_z and $I_{xy}=I_{yx}, I_{xz}=I_{zx}, I_{yz}=I_{zy}$ are elements of the inertia matrix relative to the origin of the body-fixed coordinate system defined as Equation (2.8).

$$I_0=\begin{bmatrix} I_x & -I_{xy} & -I_{xz} \\ -I_{yx} & I_y & -I_{yz} \\ -I_{zx} & -I_{zy} & I_z \end{bmatrix}, \quad I_0=I_0^T>0 \tag{2.8}$$

(2) Vectorial representation of the 6 DOF rigid-body equations of motion

Expressing the Equation (2.2) ~ (2.7) as vectors, Equation (2.7) is obtained.

$$M_{RB}\dot{\nu}+C_{RB}(\nu)\nu=\tau_{RB} \tag{2.9}$$

Here, $\nu=[u,v,r,p,q,r]^T$ is the linear velocity and angular velocity vector, $\tau_{RB}=[X,Y,Z,K,M,N]^T$ is the external force and moment vector. Matrix M_{RB} and $C_{RB}(\nu)$ are expressed by Equation (2.10) and (2.11), respectively.

$$M_{RB}=\begin{bmatrix} m & 0 & 0 & 0 & mz_G & -my_g \\ 0 & m & 0 & -mz_G & 0 & mx_G \\ 0 & 0 & m & my_G & -mx_G & 0 \\ 0 & -mz_G & my_G & I_x & -I_{xy} & -I_{xz} \\ mz_G & 0 & -mx_G & -I_{yz} & I_y & -I_{yz} \\ -my_G & mx_G & 0 & -I_{zx} & -I_{zy} & I_z \end{bmatrix} \tag{2.10}$$

$$C_{RB}(\nu)=\begin{bmatrix} 0 & 0 & 0 & m(y_Gq+z_Gr) & -m(x_Gq-w) & -m(x_Gr+v) \\ 0 & 0 & 0 & -m(y_Gp+w) & m(z_Gr+x_Gp) & -m(y_Gr-u) \\ 0 & 0 & 0 & -m(z_Gp-v) & -m(z_Gq+u) & m(x_Gp+y_Gq) \\ -m(y_Gq+z_Gr) & m(y_Gp+w) & m(z_Gp-v) & 0 & -I_{yz}q-I_{xz}p+I_zr & I_{yz}r+I_{xy}p-I_yq \\ m(x_Gq-w) & -m(z_Gr+x_Gp) & m(z_Gq+u) & I_{yz}q+I_{xz}p-I_zr & 0 & -I_{xz}r-I_{xy}q+I_xp \\ m(x_Gr+v) & m(y_Gr-u) & -m(x_Gp+y_Gq) & -I_{yz}r-I_{xy}p+I_yq & I_{xz}r+I_{xy}q-I_xp & 0 \end{bmatrix} \tag{2.11}$$

6 DOF rigid-body equations of motion can be simplified as shown in Equation (2.12) ~ (2.17) in case that origin O coincides with center of gravity, where M_{RB} and $C_{RB}(\nu)$ are expressed by Equation (2.18) and (2.19).

$$m[\dot{u}-vr+wq-x_G(q^2+r^2)+z_G(pr+\dot{q})]=X \tag{2.12}$$

$$m[\dot{v}-wp+ur+x_G(qp+\dot{r})+z_G(qr-\dot{p})]=Y \tag{2.13}$$

$$m[\dot{w}-wq+vp+x_G(rp-\dot{q})-z_G(p^2+q^2)]=N \tag{2.14}$$

$$I_x\dot{p}+(I_z-I_y)qr+m[x_Gz_G(pq+\dot{r})-z_G(\dot{v}-wp+ur)]=K \tag{2.15}$$

$$I_y\dot{q}+(I_x-I_z)rp+m[z_G(\dot{u}-vr+wq)-x_G(\dot{w}-uq+vp)+x_Gz_G(p^2-r^2)]=M \tag{2.16}$$

$$I_z\dot{r}+(I_y-I_x)pq+m[x_G(\dot{v}-wp+ur)-x_Gz_G(qr-\dot{p})]=N \tag{2.17}$$

$$M_{RB}=\begin{bmatrix} m & 0 & 0 & 0 & mz_G & 0 \\ 0 & m & 0 & -mz_G & 0 & mx_G \\ 0 & 0 & m & 0 & -mx_G & 0 \\ 0 & -mz_G & 0 & I_x & 0 & -I_{zx} \\ mz_G & 0 & -mx_G & 0 & -I_y & 0 \\ 0 & -mx_G & 0 & I_{zx} & 0 & I_z \end{bmatrix} \tag{2.18}$$

$$C_{RB}(\nu)=\begin{bmatrix} 0 & 0 & 0 & m(z_G r) & -m(x_G q-w) & -m(x_G r+v) \\ 0 & 0 & 0 & -m(w) & m(z_G r+x_G p) & -m(u) \\ 0 & 0 & 0 & -m(z_G p-v) & -m(z_G q+u) & m(x_G p) \\ -m(z_G r) & m(w) & m(z_G p-v) & 0 & -I_{xz}p+I_z r & -I_y q \\ m(x_G q-w) & -m(z_G r+x_G p) & m(z_G q+u) & I_{xz}p-I_z r & 0 & -I_{xz}r+I_x p \\ m(x_G r+v) & m(-u) & -m(x_G p) & I_y q & I_{xz}r-I_x p & 0 \end{bmatrix} \quad (2.19)$$

2.2.2 Hydrodynamic ship equation of motion

The forces and moments generated by the flow of fluid around the ship when ship is moving, consist of added forces and moments, hydrodynamic damping, restoring forces and moments. This can be expressed by Equation (2.20).

$$\tau_R = -M_A\dot{\nu} - C_A(\nu)\nu - D_P(\nu)\nu - g(\eta) \quad (2.20)$$

Here, $-M_A\dot{\nu} - C_A(\nu)\nu$ is the added mass forces, $D_P(\nu)\nu$ the potential damping, $g(\eta)$ restoring forces. In addition to potential damping, Other damping effects like skin friction, wave drift damping and damping due to vortex shedding have to be included like Equation (2.21).

$$D(\nu) = -D_P(\nu) - D_S(\nu) - D_W(\nu) - D_M(\nu) \quad (2.21)$$

Here, $D_S(\nu)$ is the skin friction, $D_W(\nu)$ the wave drift damping, $D_M(\nu)$ the damping due to vortex shedding. Therefore, hydrodynamic ship equation of motion is expressed by Equation (2.22).

$$M\dot{\nu} + C(\nu)\nu + D(\nu)\nu + g(\eta) = \tau \quad (2.22)$$

Here, $M = M_{RB} + M_A$, $C(\nu) = C_{RB}(\nu) + C_A(\nu)$ and additional mass forces and moments, hydrodynamic damping, restoring forces and moments are explained as follows.

(1) Added mass forces and moments

Added mass should be understood as pressure-induced forces and moments due to a forced harmonic motion of the body which are proportional to the acceleration of the body. It is possible to assumed that the underwater motion body which is fully submerged in the water has a fixed mass coefficient and is hardly influenced by the frequency of the wave. Under these assumptions, the fluid kinetic energy can be used to derive the added mass term, and fluid kinetic energy is expressed as the quadratic of the velocity vector of the body-fixed coordinate system. This is shown in Equation (2.23).

$$T_A = \frac{1}{2}\nu^T M_A \nu \tag{2.23}$$

Here, M_A is the 6×6 added inertia matrix.

$$M_A = -\begin{bmatrix} X_{\dot{u}} & X_{\dot{v}} & X_{\dot{w}} & X_{\dot{p}} & X_{\dot{q}} & X_{\dot{r}} \\ Y_{\dot{u}} & Y_{\dot{v}} & Y_{\dot{w}} & Y_{\dot{p}} & Y_{\dot{q}} & Y_{\dot{r}} \\ Z_{\dot{u}} & Z_{\dot{v}} & Z_{\dot{w}} & Z_{\dot{p}} & Z_{\dot{q}} & Z_{\dot{r}} \\ K_{\dot{u}} & K_{\dot{v}} & K_{\dot{w}} & K_{\dot{p}} & K_{\dot{q}} & K_{\dot{r}} \\ M_{\dot{u}} & M_{\dot{v}} & M_{\dot{w}} & M_{\dot{p}} & M_{\dot{q}} & M_{\dot{r}} \\ N_{\dot{u}} & N_{\dot{v}} & N_{\dot{w}} & N_{\dot{p}} & N_{\dot{q}} & N_{\dot{r}} \end{bmatrix} \tag{2.24}$$

As M_A is represented by the SNAME notation, for example the hydrodynamic added mass force along the y-axis due to an acceleration $\dot{u}$ in the x-direction is written as Equation (2.25).

$$Y = -Y_{\dot{u}}\dot{u} \tag{2.25}$$

where, $Y_{\dot{u}} = \frac{\partial Y}{\partial \dot{u}}$

The hydrodynamic coriolis matrix is given by Equation (2.26).

$$C_A(\nu) = \begin{bmatrix} 0 & 0 & 0 & 0 & -a_3 & a_2 \\ 0 & 0 & 0 & a_3 & 0 & -a_1 \\ 0 & 0 & 0 & -a_2 & a_1 & 0 \\ 0 & -a_3 & a_2 & 0 & -b_3 & b_2 \\ a_3 & 0 & -a_1 & b_3 & 0 & -b_1 \\ -a_2 & a_1 & 0 & -b_2 & b_1 & 0 \end{bmatrix} \tag{2.26}$$

Here, a_1, a_2, a_3, b_1, b_2 and b_3 are written as Equation (2.27).

$$\begin{aligned} a_1 &= X_u u + X_v v + X_w w + X_p p + X_q q + X_r r \\ a_2 &= X_u u + Y_v v + Y_w w + Y_p p + Y_q q + Y_r r \\ a_3 &= X_u u + Y_v v + Z_w w + Z_p p + Z_q q + Z_r r \\ b_1 &= X_u u + Y_v v + Z_w w + K_p p + K_q q + K_r r \\ b_2 &= X_u u + Y_v v + Z_w w + K_p p + M_q q + M_r r \\ b_3 &= X_u u + Y_v v + Z_w w + K_p p + M_q q + N_r r \end{aligned} \tag{2.27}$$

The hydrodynamic inertial matrix M_A and coriolis matrix $C_A(\nu)$ also can be simplified if the ship is bilaterally symmetric, that is, when ship is symmetric to the xz-plane. M_A and $C_A(\nu)$ are written as Equation (2.28) and Equation (2.29).

$$M_A = -\begin{bmatrix} X_{\dot{u}} & 0 & X_{\dot{w}} & 0 & X_{\dot{q}} & 0 \\ 0 & Y_{\dot{v}} & 0 & Y_{\dot{p}} & 0 & Y_{\dot{r}} \\ Z_{\dot{u}} & 0 & Z_{\dot{w}} & 0 & Z_{\dot{q}} & 0 \\ 0 & Y_{\dot{v}} & 0 & K_{\dot{p}} & 0 & K_{\dot{r}} \\ X_{\dot{u}} & 0 & Z_{\dot{w}} & 0 & M_{\dot{q}} & 0 \\ 0 & Y_{\dot{v}} & 0 & K_{\dot{p}} & 0 & N_{\dot{r}} \end{bmatrix} \tag{2.28}$$

$$C_A(\nu)=\begin{bmatrix} 0 & 0 & 0 & 0 & -a_3 & a_2 \\ 0 & 0 & 0 & a_3 & 0 & -a_1 \\ 0 & 0 & 0 & -a_2 & a_1 & 0 \\ 0 & -a_3 & a_2 & 0 & -b_3 & b_2 \\ a_3 & 0 & -a_1 & b_3 & 0 & -b_1 \\ -a_2 & a_1 & 0 & -b_2 & b_1 & 0 \end{bmatrix} \tag{2.29}$$

Here, a_1, a_2, a_3, b_1, b_2 and b_3 are written as Equation (2.30).

$$\begin{aligned} a_1 &= X_u u + X_w w + X_q q \\ a_2 &= Y_v v + Y_p p + Y_r r \\ a_3 &= X_u u + Z_w w + Z_q q \\ b_1 &= Y_v v + K_p p + K_r r \\ b_2 &= X_u u + Z_w w + M_q q \\ b_3 &= Y_v v + K_p p + N_r r \end{aligned} \tag{2.30}$$

(2) Hydrodynamic damping

Hydrodynamic damping consists of potential damping, damping by skin friction, wave drift damping and damping due to vortex shedding is written as Equation (2.31).

$$D(\nu) = D_P(\nu) + D_S(\nu) + D_W(\nu) + D_M(\nu) \tag{2.31}$$

Here, $D_S(\nu)$ is damping by skin friction, $D_W(\nu)$ wave drift damping and $D_M(\nu)$ damping due to vortex shedding. The damping model is classified into damping model of DP ship and damping model of high speed maneuvering ship.

1) Damping model of DP ship

The equation of motion of DP ship can be divided into the forward speed equation and the steering equation because the aim of DP ship is to maintain the position. Ignoring heave, roll and pitch motion, Damping matrix of the DP ship can be expressed by Equation (2.32).

$$D = -\begin{bmatrix} X_u & 0 & 0 \\ 0 & Y_v & Y_r \\ 0 & N_v & N_r \end{bmatrix} \tag{2.32}$$

2) Damping model of high speed maneuvering ship

Damping model of high speed maneuvering ship is proposed by Blanke and includes the nonlinear coupling term.

$$D(\nu) = -\begin{bmatrix} X_{|u|u}|u| & 0 & 0 \\ 0 & Y_{|v|v}|v| + Y_{|r|v}|r| & Y_{|v|r}|v| + Y_{|r|r}|r| \\ 0 & N_{|v|v}|v| + N_{|r|v}|r| & N_{|v|r}|v| + N_{|r|r}|r| \end{bmatrix} \tag{2.33}$$

In case of large ship, $|r|r$ and $|r|v$ are very small and negligible, so that the damping model is written as Equation (2.34).

$$D(\nu) = -\begin{bmatrix} X_{|u|u}|u| & 0 & 0 \\ 0 & Y_{|v|v}|v| & Y_{|v|r}|v| \\ 0 & N_{|v|v}|v| & N_{|v|r}|v| \end{bmatrix} \tag{2.34}$$

In this paper, Equation (2.34) is used as damping model because the ship used for the simulation is a cargo ship which can be considered as a large ship.

3) Restoring forces and moments

Restoring forces depend on the shape and size of the ship, the height of the metacentric center, and the location of the center of gravity and the center of the buoyancy. The restoring force and moment matrix are written as Equation (2.35).

$$g(\eta)=\begin{bmatrix} -\rho g\int_0^z A_{wp}(\zeta)d\zeta\sin\theta \\ \rho g\int_0^z A_{wp}(\zeta)d\zeta\cos\theta\sin\phi \\ \rho g\int_0^z A_{wp}(\zeta)d\zeta\cos\theta\cos\phi \\ \rho g\nabla\ \overline{GM_T}\sin\phi\cos\theta\cos\phi \\ \rho g\nabla\ \overline{GM_L}\sin\theta\cos\theta\cos\phi \\ \rho g\nabla\ (-\overline{GM_T}-\overline{GM_L})\sin\phi\sin\theta \end{bmatrix} \tag{2.35}$$

Here, $\eta=[x,y,z,\phi,\theta,\psi]^T$ is position and Euler angles, ρ is water density, g is gravitation acceleration, ∇ is displacement and $A_{wp}(\zeta)$ is the horizontal area of the ship expressed as a function of vertical position. The restoring forces and moments can be ignored if the ship is stable.

2.3 3 DOF nonlinear ship equation of motion

The ship maneuvering on sea is symmetric in xz plane, and its equation of motion can be separated into the forward direction speed equation and the steering motion equation. Assuming that the below four conditions are satisfied and restoring force are ignored, a nonlinear ship equation of motion can be derived consisting of the motion in the x-direction, the motion in the y-direction and the rotational motion about z-axis [5].

1) The ship motion can be separated into the speed equation and steering motion equation.
2) The ship's heave, roll, and pitch motion component are negligible.
3) The origin of the body fixed coordinate system is located at the center line of the ship.
4) The ship is symmetrical in xz plane.

$$M\dot{\nu} + C(\nu)\nu + D\nu = \tau \tag{2.36}$$

Here, vector $\nu = [u, v, r]^T$ and $M, C(\nu)$ and D are written as Equation (2.37).

$$M = \begin{bmatrix} m - X_{\dot{u}} & 0 & 0 \\ 0 & m - Y_{\dot{v}} & mx_G - Y_{\dot{r}} \\ 0 & mx_G - N_{\dot{r}} & I_z - N_{\dot{r}} \end{bmatrix}$$

$$C(\nu) = \begin{bmatrix} 0 & 0 & -(m - Y_{\dot{v}})v + (mx_G - Y_{\dot{r}})r \\ 0 & 0 & (m - X_{\dot{u}})u \\ (m - Y_{\dot{v}})v + (mx_G - Y_{\dot{r}})r - (m - X_{\dot{u}})u & 0 \end{bmatrix} \tag{2.37}$$

$$D = \begin{bmatrix} -X_u & 0 & 0 \\ 0 & -Y_v & -Y_r \\ 0 & -N_v & -N_r \end{bmatrix}$$

2.3.1 Separation of speed equation and steering equation

If the ship is maneuvering at a constant speed and speed change is small, the speed of the ship is approximated to the forward direction speed $U = \sqrt{u^2 + v^2} \approx u$. At this time, the 3 DOF nonlinear ship model can be separated into forward direction speed model and steering model.

1) Forward direction speed model

The forward direction speed model is written as Equation (2.38).

$$(m - X_{\dot{u}})\dot{u} - X_u u - X_{|u|u}|u|u = \tau_s \tag{2.38}$$

Here, τ_s is the sum of the forward direction control force.

2) 2 DOF linear steering model

The 2 DOF linear steering model can be obtained under the assumption that the ship's forward direction speed u is constant, and the lateral speed v and angular velocity r are very small. Therefore, The condition of $u \approx u_0$, $v \approx 0$ and $r \approx 0$ must be satisfied, and the 2 DOF linear steering model is written as Equation (2.39).

$$M\dot{\nu} + C(\nu)\nu + D\nu = \tau \tag{2.39}$$

Here, vector $\nu = [v, r]^T$, $M, C(\nu)$ and D is written as Equation (2.40). If the ship is controlled by a single steering gear, then τ is written as Equation (2.41).

$$M = \begin{bmatrix} m - Y_{\dot{v}} & mx_G - Y_{\dot{r}} \\ mx_G - Y_{\dot{r}} & I_z - N_{\dot{r}} \end{bmatrix}$$

$$C(\nu) = \begin{bmatrix} 0 & (m - X_{\dot{u}})u_0 \\ (X_{\dot{u}} - Y_{\dot{v}})u_0 & (mx_G - Y_{\dot{r}})u_0 \end{bmatrix} \tag{2.40}$$

$$D = \begin{bmatrix} -Y_v - Y_r \\ -N_v - N_r \end{bmatrix}$$

$$\tau = \begin{bmatrix} -Y_\delta \\ -N_\delta \end{bmatrix} \delta \tag{2.41}$$

2.4 Linearlization on 3 DOF nonlinear ship equation of motion

If the ship's forward direction speed is constant and the lateral direction speed and angular velocity are very small, it is possible to separate into forward direction motion and steering motion. In this section, we examine the linear forward direction speed model proposed by Blanke and the linear steering motion model proposed by Davidson and Schiff. The rigid body 3

DOF nonlinear ship equation of motion is written as Equation (2.42).

$$M_{RB}\dot{\nu} + C_{RB}(\nu)\nu = \tau_{RB} \tag{2.42}$$

Here, $\tau_{RB} = [X, Y, N]^T$ means force and moment, M_{RB} and $C_{RB}(\nu)$ are written as Equation (2.43).

$$M_{RB} = \begin{bmatrix} m & 0 & 0 \\ 0 & m & mx_G \\ 0 & mx_G & I_z \end{bmatrix} \; C_{RB} = \begin{bmatrix} 0 & 0 & -m(x_G r + v) \\ 0 & 0 & mu \\ m(x_G r + v) & -mu & 0 \end{bmatrix} \tag{2.43}$$

By substituting τ_{RB} and Equation (2.43) into Equation (2.42), 3 DOF nonlinear ship equation of motion can be expressed as surge, sway, and yaw equation as shown in Equation (2.44).

$$\begin{aligned} &surge : m(\dot{u} - vr - x_G r^2) = X \\ &sway : m(\dot{v} + ur + x_G \dot{r}) = Y \\ &yaw : \; I_z \dot{r} + mx_G(\dot{v} + ur) = N \end{aligned} \tag{2.44}$$

The linearization of Equation (2.44) can be achieved from the assumption that the ship has constant value in the forward direction speed $U \approx u_0$, has a very small value at the lateral speed $v \approx 0$, angular velocity $r \approx 0$. Therefore the linear approximated 3 DOF equations of motion are written as Equation (2.45).

$$\begin{aligned} &surge : m\dot{u}_0 = X \\ &sway : m(\dot{v} + u_0 r + x_G \dot{r}) = Y \\ &yaw : \; I_z \dot{r} + mx_G(\dot{v} + u_0 r) = N \end{aligned} \tag{2.45}$$

2.4.1 Linear forward direction motion model proposed by Blanke

Ship's forward direction motion is related to propeller thrust and forward direction speed. Blanke proposed a hydrodynamic force consisting of a nonlinear function as Equation (2.46).

$$X = X_{\dot{u}}\dot{u} + X_{vr}vr + X_{|u|u}|u|u + X_{rr}r^2 + (1-t)T + X_{cc\delta\delta}c^2\delta^2 + X_{ext} \tag{2.46}$$

By substituting Equation (2.46) into surge equation of Equation (2.43), the forward direction equation of motion is finally expressed by Equation (2.47).

$$\begin{aligned} (m - X_{\dot{u}})\dot{u} &= X_{|u|u}|u|u + (1-t)T + T_{loss} \\ T_{loss} &= (m + X_{vr})vr + X_{cc\delta\delta}c^2\delta^2 + (X_{rr} + mx_G)r^2 + X_{ext} \end{aligned} \tag{2.47}$$

Here, Hydrodynamic coefficients are shown in Table 2.2.

Table 2.2 Hydrodynamic coefficients

$X_{\dot{u}}$	added mass in surge
$X_{\|u\|u}$	drag force coefficient in surge
t	thrust deduction number
$X_{cc\delta\delta}$	resistance due to rudder deflection
T	propeller thrust
c	flow velocity past the rudder
T_{loss}	loss term or added resistance
$(m + X_{vr})$	excessive drag force due to combined swat-yaw motion
$(X_{rr} + mx_G)$	excessive drag force in yaw
X_{ext}	external force due to wind and wave

Because the drag force and propeller thrust are more dominant than T_{loss} when ship is in a steady state, T_{loss} can be assumed to be zero. Thus, the linearized forward direction motion model, Equation (2.48), can be obtained.

$$(m-X_{\dot{u}})\dot{u}=X_{|u|u}|u|u+(1-t)T \tag{2.48}$$

Expressing Equation (2.48) as a state equation, Equation (2.49) is obtained.

$$\dot{u}=\frac{X_{|u|u}|u|}{(m-X_{\dot{u}})}u+\frac{(1-t)}{(m-X_{\dot{u}})}T \tag{2.49}$$

Here, $\frac{X_{|u|u}|u|}{(m-X_{\dot{u}})}$ and $\frac{(1-t)}{(m-X_{\dot{u}})}$ are defined as c and d, respectively. And c,d is used to create the state space equation of ship later.

2.4.2 Linear steering equation suggested by Davison and Schiff

It is shown that ship's linear steering model can be separated from linear forward direction motion model on the assumption that the forward direction speed is constant, the lateral speed and the angular velocity are very small. Thus the steering model is expressed as only functions of the lateral speed v, the angular velocity r, heading angle and the control input for rudder angle δ. In this case Davidson and Schiff proposed hydrodynamic forces and moments as Equation (2.50).

$$\begin{aligned} Y&=Y_{\dot{v}}\dot{v}+Y_{\dot{r}}\dot{r}+Y_v v+Y_r r+Y_\delta\delta \\ N&=N_{\dot{v}}\dot{v}+N_{\dot{r}}\dot{r}+N_v v+N_r r+N_\delta\delta \end{aligned} \tag{2.50}$$

By substituting Equation (2.50) into sway, yaw equation of Equation (2.44), the linear steering equation can be expressed by a vector model such as Equation (2.51).

$$M\dot{\nu} + N(u)\nu = b\delta_R \tag{2.51}$$

Here, $\nu = [v, r]^T$ is state vector, δ_R is rudder angle, $M, N(u)$ and b are expressed as Equation (2.52).

$$M = \begin{bmatrix} m - Y_{\dot{v}} & mx_G - Y_{\dot{r}} \\ mx_G - Y_{\dot{r}} & I_Z - N_{\dot{r}} \end{bmatrix}$$
$$N(u) = \begin{bmatrix} -Y_v & mu - Y_r \\ -N_v & mx_G u - N_r \end{bmatrix} b = \begin{bmatrix} Y_\delta \\ N_\delta \end{bmatrix} \tag{2.52}$$

Here, $Y_{\dot{v}}$ and $N_{\dot{v}}$ are the added mass and moment due to fluid motion, Y_v, Y_δ, N_r and N_δ are the Hydrodynamic coefficients. Defining the vector model of the linearized steering motion model as state vector $x_s = [v, r]^T$ and $u = \delta$, the resultant state equation can be obtained as Equation (2.53).

$$\dot{x_s} = A_s x_s + B_s u \tag{2.53}$$

Here, A_s, B_s is written as Equation (2.54).

$$A_s = -M^{-1}N(u) = \begin{bmatrix} a_{11} & a_{12} \\ a_{21} & a_{22} \end{bmatrix}$$
$$B_s = M^{-1}b = \begin{bmatrix} b_1 \\ b_2 \end{bmatrix} \tag{2.54}$$

Here, Each element $a_{11}, a_{12}, a_{21}, a_{22}, b_1$ and b_2 of A_s and B_s matrix is given by Equation (2.55).

$$a_{11} = \frac{-(I_z - N_{\dot{r}})Y_v + (mx_G - Y_{\dot{r}})N_v}{\det(M)}$$

$$a_{12} = \frac{(I_z - N_{\dot{r}})(\mu_0 - Y_r) - (mx_G - Y_{\dot{r}})(mx_G u_0 - N_{\dot{r}})}{\det(M)}$$

$$a_{21} = \frac{-(m - Y_{\dot{v}})N_v + (mx_G - N_{\dot{v}})Y_v}{\det(M)}$$

$$a_{22} = \frac{(m - Y_{\dot{v}})(mx_G u_0 - N_{\dot{r}}) - (mx_G u_0 - N_r)(m u_0 - Y_r)}{\det(M)} \quad (2.55)$$

$$b_1 = \frac{-(I_z - N_{\dot{r}})Y_\delta + (mx_G - Y_{\dot{r}})N_\delta}{\det(M)}$$

$$b_2 = \frac{-(m - Y_{\dot{v}})N_\delta + (mx_G - N_{\dot{v}})Y_\delta}{\det(M)}$$

$$\det(M) = (m - Y_{\dot{v}})(I_z - N_{\dot{r}}) - (mx_G - N_{\dot{v}})(mx_G - Y_{\dot{r}}) > 0$$

2.5 Combination of linear speed equation with liner steering equation

The linear 3 DOF ship equation of motion can be obtained by combining the linearized forward direction speed model with the linearized steering motion model of Section 2.4. Expressing the 3 DOF ship equation of motion as a state equation, equation (2.56) is obtained by defining $x = [u, v, r]^T$ and $u = [T, \delta]^T$.

$$\dot{x} = Ax + Bu$$

$$A = \begin{bmatrix} c & 0 & 0 \\ 0 & a_{11} & a_{12} \\ 0 & a_{21} & a_{22} \end{bmatrix}, B = \begin{bmatrix} d & 0 \\ 0 & b_1 \\ 0 & b_2 \end{bmatrix} \quad (2.56)$$

On the other hand, the speed of the ship and the angular velocity of the ship based on the earth fixed coordinate system can be obtained by the speed transformation given as Equation (2.57). Therefore, by combining

Equation (2.56) with Equation (2.57), it is possible to establish a state equation like Equation (2.58), which can represent the position, and velocity of a ship. At this time, the state vector x and u are defined as $[x,y,\psi,u,v,r]^T$ and $[T,\delta]^T$ respectively.

$$\begin{bmatrix}\dot{x}\\ \dot{y}\\ \dot{\psi}\end{bmatrix}=\begin{bmatrix}\cos\psi & -\sin\psi & 0\\ \sin\psi & \cos\psi & 0\\ 0 & 0 & 1\end{bmatrix}\begin{bmatrix}u\\ v\\ r\end{bmatrix} \tag{2.57}$$

$$\dot{x}=Ax+Bu$$

$$A=\begin{bmatrix}0&0&0&\cos\psi & -\sin\psi & 0\\ 0&0&0&\sin\psi & \cos\psi & 0\\ 0&0&0&0 & 0 & 1\\ 0&0&0&c & 0 & 0\\ 0&0&0&0 & a_{11} & a_{12}\\ 0&0&0&0 & a_{21} & a_{22}\end{bmatrix},\ B=\begin{bmatrix}0&0\\ 0&0\\ 0&0\\ d&0\\ 0&b_1\\ 0&b_2\end{bmatrix} \tag{2.58}$$

x and y are the ship position and ψ is the heading angle in the earth fixed coordinate system. And the x-direction is normally north.

2.6 Simulation on path following of ship

2.6.1 Simulation condition

The ship model used in the simulation is obtained by discretizing Equation (2.58) by Euler discretization method and zero-order hold technique. The specifications of the ship are shown in Table 2.3, and the forward speed of the ship is set to $8m/s$.

Table 2.3 Specifications of a cargo ship

$L(m)$	171.8
$L_{pp}(m)$	160.93
$\nabla\ (m^3)$	18541
$B(m)$	23.17
$Draft(m)$	8.23

Here, L is ship length, L_{pp} is length between perpendiculars, ∇ is design displacement and B is maximum beam. The PD controller given as Equation (2.59) is used as the heading angle keeping controller and control parameter are set to $K_p = 1, K_d = 70$ as optimal. The stability of the ship is assured by limiting the rudder angle to $\pm 20^{\circ}$ in order to prevent the ship from becoming unstable due to sudden turning.

$$\delta = -K_p(\psi_d - \psi) + K_d r \tag{2.59}$$

Here, ψ_d is the reference heading angle, ψ heading angle and r angular velocity. In an actual environment, environment disturbances such as current, wave and wind are applied to the ship as unknown disturbances, which interfere with the ship motion. But, in this discuss, simulations are performed only to show the ship motion in order to verified path following of ship based on linear 3 DOF equation of motion without applying unknown disturbances. Simulations with unknown disturbances will be described in chapter 4.

2.6.2 Simulation results of path following (PD autopilot)

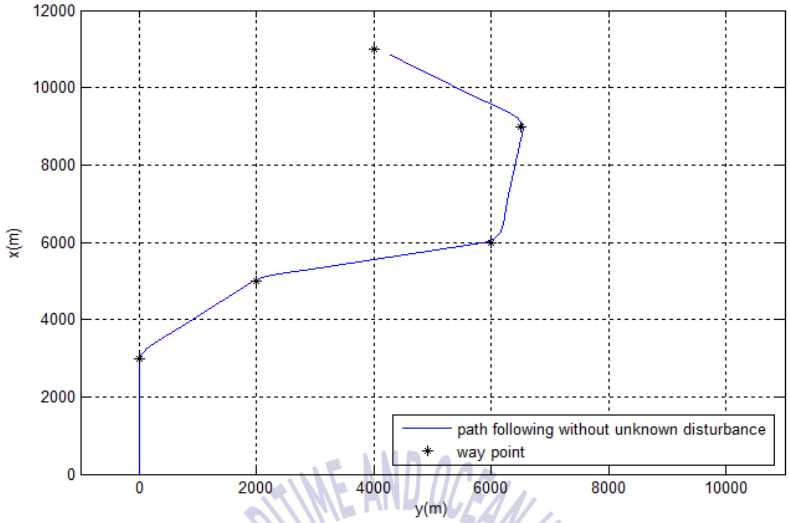

Fig. 2.2 Path following without unknown disturbances

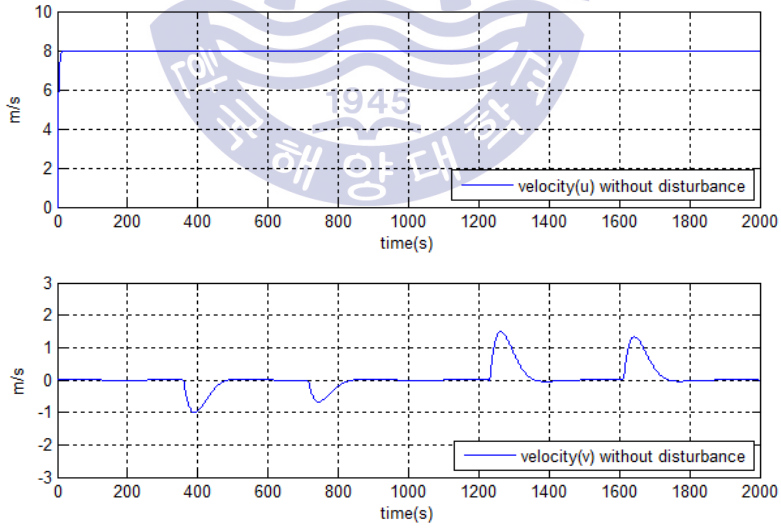

Fig. 2.3 Velocity u and v without unknown disturbances

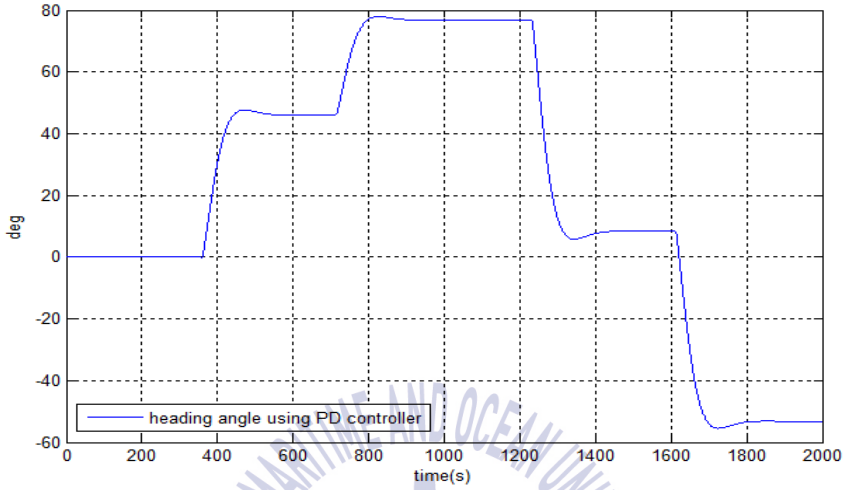

Fig. 2.4 Heading angle ψ without unknown disturbances

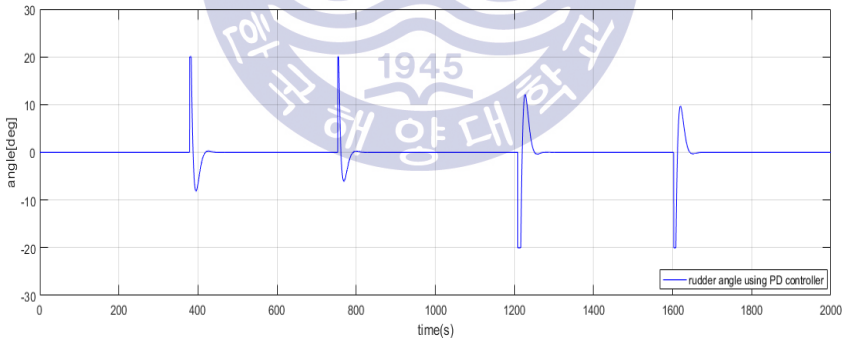

Fig. 2.5 Rudder angle

Fig. 2.2 shows a simulation result for path following of ship using PD autopilot system as a heading angle keeping controller. As seen in the figure, the ship does not deviate much from the desired route and follows the route closely. Fig. 2.2 is simulation result for the ship forward speed and lateral speed. From the figures, it can be seen that the forward direction speed is maintained at the initial set value $8m/s$ and lateral speed also does not appear in the range except altering the course. Fig. 2.4 is a simulation result showing the heading angle controlled by PD autopilot system. Since the PD controller is used as the autopilot, overshoot can be occurred and the ship can be expected to deviate from the defined route. Figure 2.5 shows the rudder angle when the ships alters course by the PD type autopilot system, so that the rudder angle is changed roughly and it cause to increase the energy loss of the ship. In order to improve the limit of PD autopilot, chapter 3 describes velocity type fuzzy PID autopilot system.

Chapter 3 Velocity type fuzzy PID autopilot system

PD controller with simple structure has been used as an autopilot system to control the heading of ship. Although the PD autopilot system has the ability to adjust the response speed, stabilization, and overshoot, overshoot is inevitably occurred whenever the course change angle is large, which causes the energy loss of the ship. Also, there is a limitation when the nonlinearity is strong. In chapter 3, a velocity type fuzzy PID autopilot is developed to improve the limit of PD autopilot. It has the ability to adapt strong nonlinearity and does not exhibit overshoot in spite of abrupt large course change. Fuzzy PID system is divided into two type, one of which is position type and the other is velocity type. In this paper, in order to determine the control input, velocity type fuzzy PID autopilot is applied, because position type fuzzy PID autopilot system that directly decide the value of control input can not be used in the ship applications [8][10].

3.1 Velocity type fuzzy PID autopilot system

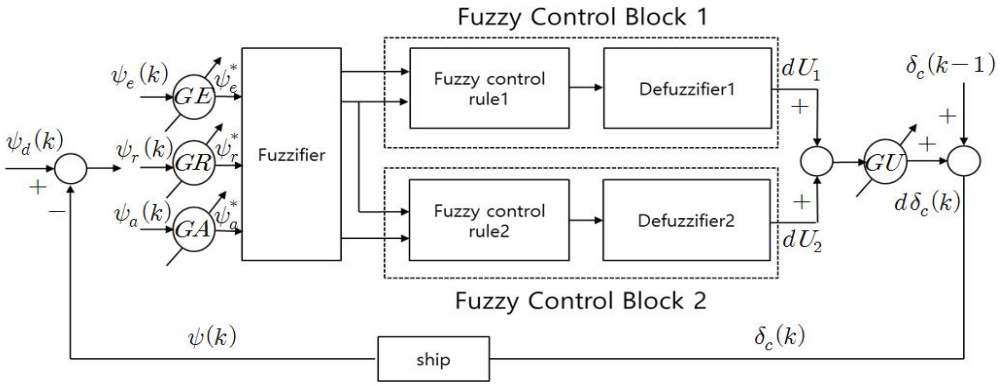

Fig. 3.1 Functional diagram of velocity type fuzzy PID autopilot

Fig. 3.1 shows the structure of velocity type fuzzy PID autopilot composed of two different fuzzy control blocks including fuzzy control rules and defuzzifiers, respectively. Fuzzy PID controller uses the value of heading angle error, speed of error and acceleration of error as its inputs and it generates the control increment of rudder angle as an output [17].

$$
\begin{aligned}
&\psi_e(k) = \psi_d(k) - \psi(k) \\
&\psi_e^* = GE \times \psi_e(k) \\
&\psi_r(k) = [\psi_e(k) - \psi_e(k-1)]/T \\
&\psi_r^* = GR \times \psi_r(k) \\
&\psi_a(k) = [\psi_r(k) - \psi_r(k-1)]/T \\
&\psi_a^* = GA \times \psi_a(k)
\end{aligned}
\tag{3.1}
$$

$$
\begin{aligned}
&dU = dU_1 + dU_2 \\
&d\delta_c(k) = GU \times dU,\ \delta_c(k) = d\delta_c(k) + \delta_c(k-1)
\end{aligned}
\tag{3.2}
$$

Here, T is the sampling time, $\psi(k), \psi_e(k), \psi_r(k)$ and $\psi_a(k)$ is respectively heading angle, heading angle error, change rate of heading angle error, change rate of time of heading angle of ship in sampling time k. GE, GR, GA and GU is respectively parameters in fuzzification scale of $\psi_e^*, \psi_r^*, \psi_a^*$ and $d\delta_c(k)$. GU is used to calculate the total control gain of fuzzy PID controller. dU_1 and dU_2 are the output of fuzzy control block 1 and 2. δ_c means rudder command angle as a control input. The next thing is how to fuzzify $\psi_e^*, \psi_r^*, \psi_a^*$ into fuzzy sets for the inputs of velocity type fuzzy PID autopilot. The specific contents about designing the general fuzzy PID control system is addressed in [12].

3.1.1 Fuzzification algorithm

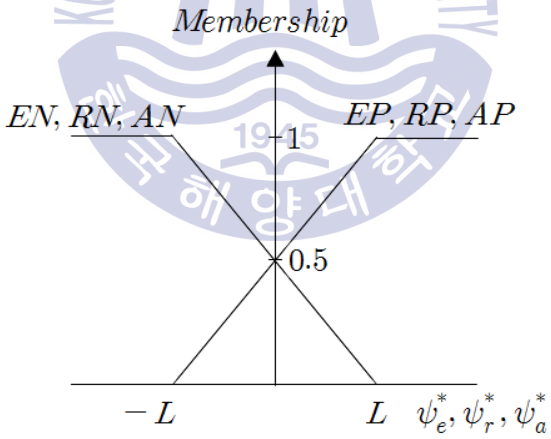

Fig. 3.2 Fuzzification of ψ_e^*, ψ_r^* and ψ_a^*

Fig. 3.2 shows fuzzification algorithms of ψ_e^*, ψ_r^* and ψ_a^* mapping into fuzzy sets. ψ_e^* is mapped into two fuzzy sets of EP and EN. ψ_r^* is mapped into two fuzzy sets of RP and RN. And ψ_a^* is mapped into two fuzzy sets of AP and AN.

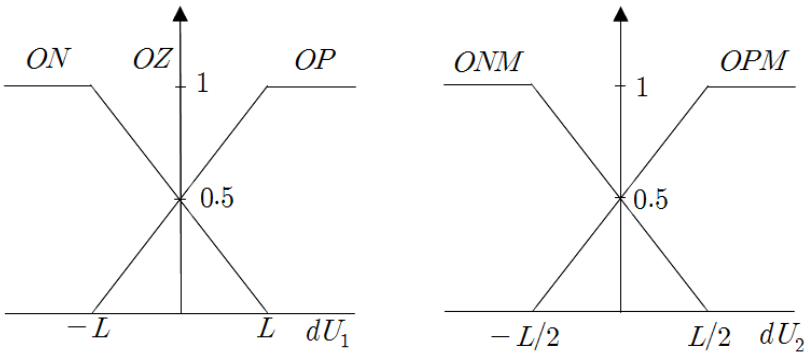

Fig. 3.3 Output fuzzification for fuzzy control block 1 and 2

The fuzzy output for dU_1 is shown in the left figure of Fig. 3.3, and has three fuzzy sets as OP, OZ and ON. The fuzzy output for dU_2 is shown in the right figure of Fig. 3.3, and has two fuzzy sets as OPM and ONM.

3.1.2 Fuzzy control rule

Fuzzy control rules are created in the form of conditional statements and the control rules for fuzzy control blocks 1 and 2 are as follows [11].

Fuzzy control block 1
$(R1)_1 : IF\ \psi_e^* = EP$ and $\psi_r^* = RP\ \ THEN\ \ dU_1 = OP$
$(R2)_1 : IF\ \psi_e^* = EP$ and $\psi_r^* = RN\ \ THEN\ \ dU_1 = OZ$
$(R3)_1 : IF\ \psi_e^* = EN$ and $\psi_r^* = RP\ \ THEN\ \ dU_1 = OZ$
$(R4)_1 : IF\ \psi_e^* = EN$ and $\psi_r^* = RN\ \ THEN\ \ dU_1 = ON$
Fuzzy control block 2
$(R1)_2 : IF\ \psi_r^* = RP$ and $\psi_a^* = AP\ THEN\ \ dU_2 = OPM$
$(R2)_2 : IF\ \psi_r^* = RP$ and $\psi_a^* = AN\ THEN\ \ dU_2 = ONM$
$(R3)_2 : IF\ \psi_r^* = RN$ and $\psi_a^* = AP\ THEN\ \ dU_2 = OPM$
$(R4)_2 : IF\ \psi_r^* = RN$ and $\psi_a^* = AN\ THEN\ \ dU_2 = ONM$

The control rules of fuzzy control block 1 and 2 are applied with the AND logic of Zadeh for the premise parts, which performs a min operation to find the fitness of the consequent parts of the control rules.

$$IF\ GE \times |\psi_e(k)| > L\ THEN\ GE = L/|\psi_e(k)| \tag{3.3}$$

$$IF\ GR \times |\psi_r(k)| > L\ THEN\ GR = L/|\psi_r(k)|,\ GU = 4/GR \tag{3.4}$$

$$IF\ GA \times |\psi_a(k)| > L\ THEN\ GA = L/|\psi_a(k)| \tag{3.5}$$

The scale parameters GE and GR are varied with the consequent parts whenever the conditions of Equation (3.3) and Equation (3.4) are satisfied. Since the overall gain of the controller must always be constant, GU is changed at the same time whenever GR is varied. GA is also changed with consequent part, whenever the condition of Equation (3.5) is satisfied. Because of this variable GE, GR, GA and GU, the input spaces for fuzzy control blocks 1 and 2 are divided into $(IC1)_1$ ~ $(IC8)_1$ and $(IC1)_2$ ~ $(IC8)_2$ respectively in the interval $[-L, L]$ as shown in Fig. 3.4 and Fig. 3.5.

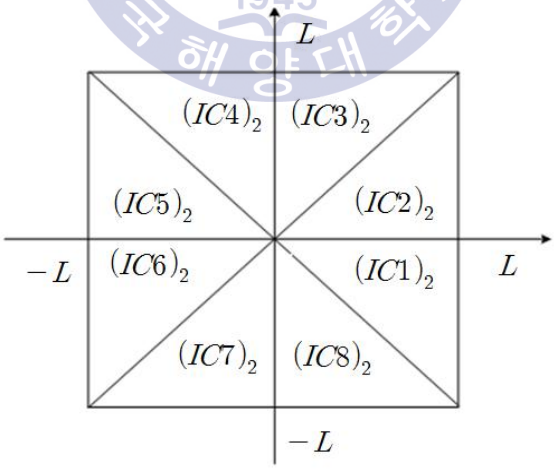

Fig. 3.4 Possible input partition combinations of $\psi_e^*$and ψ_r^* using fixed normalization parameter L for fuzzy control block 1

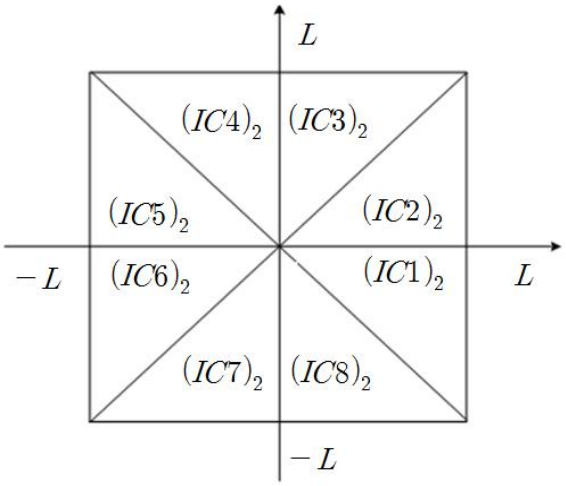

Fig. 3.5 Possible input partition combinations of $\psi_r^*$and ψ_a^* using fixed normalization parameter L for fuzzy control block 2

The control increment $d\delta_c(k)$, which is the output of the fuzzy PID controller through defuzzification, where the weighted center method is used for the defuzzification [11]. The resultant control algorithm of the velocity type fuzzy PID autopilot is summarized as following equations.

1)

IF $GR \times |\psi_r(k)| \le GE \times |\psi_e(k)| \le L$ and $GA \times |\psi_a(k)| \le GR \times |\psi_r(k)| \le L$,

THEN

$$d\delta_c(k) = \frac{0.5 \times L \times GU \times GE}{2L - GE \times |\psi_e(k)|}\psi_e(k) + \frac{0.5 \times L \times GU \times GR}{2L - GE \times |\psi_e(k)|}\psi_r(k)$$

$$+ \frac{0.25 \times L \times GU \times GA}{2L - GR \times |\psi_r(k)|}\psi_a(k) \tag{3.6}$$

2)

IF $GR \times |\psi_r(k)| \leq GE \times |\psi_e(k)| \leq L$ and $GR \times |\psi_a(k)| \leq GA \times |\psi_r(k)| \leq L$,

THEN

$$d\delta_c(k) = \frac{0.5 \times L \times GU \times GE}{2L - GE \times |\psi_e(k)|}\psi_e(k) + \frac{0.5 \times L \times GU \times GR}{2L - GE \times |\psi_e(k)|}\psi_r(k) + \frac{0.25 \times L \times GU \times GA}{2L - GA \times |\psi_r(k)|}\psi_a(k) \tag{3.7}$$

3)

IF $\geq \times |\psi_e(k)| \leq GR \times |\psi_r(k)| \leq L$ and $GR \times |\psi_a(k)| \leq GA \times |\psi_r(k)| \leq L$,

THEN

$$d\delta_c(k) = \frac{0.5 \times L \times GU \times GE}{2L - GR \times |\psi_r(k)|}\psi_e(k) + \frac{0.5 \times L \times GU \times GR}{2L - GR \times |\psi_r(k)|}\psi_r(k) + \frac{0.25 \times L \times GU \times GA}{2L - GA \times |\psi_r(k)|}\psi_a(k) \tag{3.8}$$

4)

IF $\geq \times |\psi_e(k)| \leq GR \times |\psi_r(k)| \leq L$ and $GR \times |\psi_r(k)| \leq GA \times |\psi_a(k)| \leq L$,

THEN

$$d\delta_c(k) = \frac{0.5 \times L \times GU \times GE}{2L - GR \times |\psi_r(k)|}\psi_e(k) + \frac{0.5 \times L \times GU \times GR}{2L - GR \times |\psi_r(k)|}\psi_r(k) + \frac{0.25 \times L \times GU \times GA}{2L - GR = A \times |\psi_a(k)|}\psi_a(k) \tag{3.9}$$

3.2 Performance verification of velocity type fuzzy PID autopilot

Simulation are accomplished to compare the performance of velocity type fuzzy PID autopilot system with that of PD type autopilot system for the course change angle $30^\circ, 45^\circ$ and 60°. The specification of the ship is shown in Table 2.3, and the gain of the PD controller is optimized to $K_p = 1, K_d = 70$. The rudder angle is limited to $\pm 20^\circ$ to assure the stability of the ship.

3.2.1 Course change simulation

(1) When the course change angle is 30[deg]

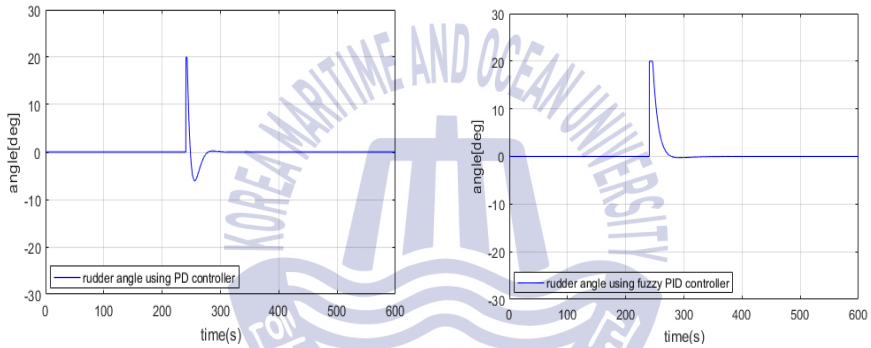

Fig. 3.6 Comparison of rudder angles using PD and fuzzy PID autopilot

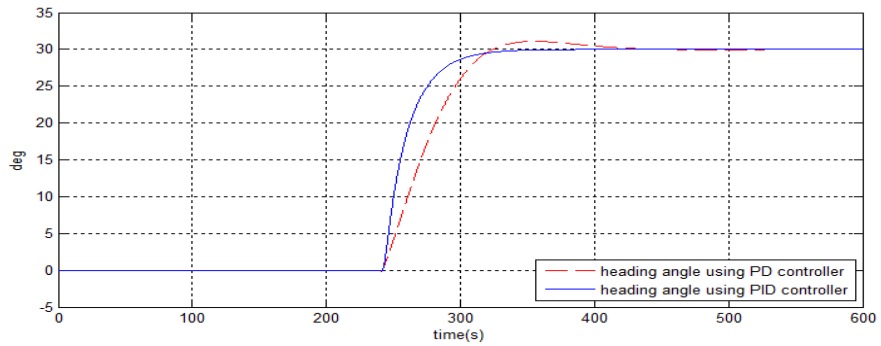

Fig. 3.7 Comparison of heading angles using PD and fuzzy PID autopilot

(2) When the course change angle is 45[deg]

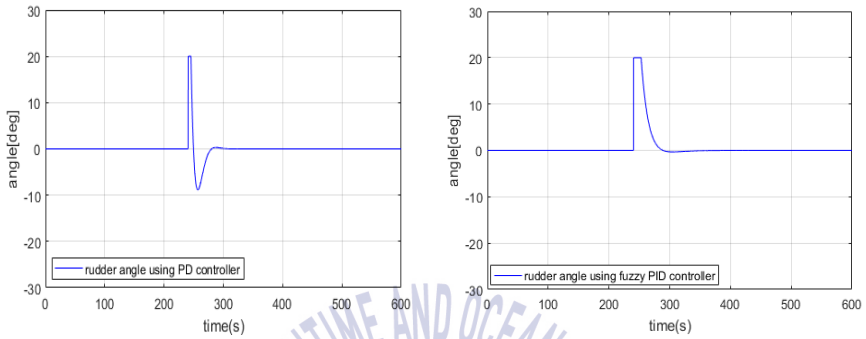

Fig. 3.8 Comparison of rudder angles using PD and fuzzy PID autopilot

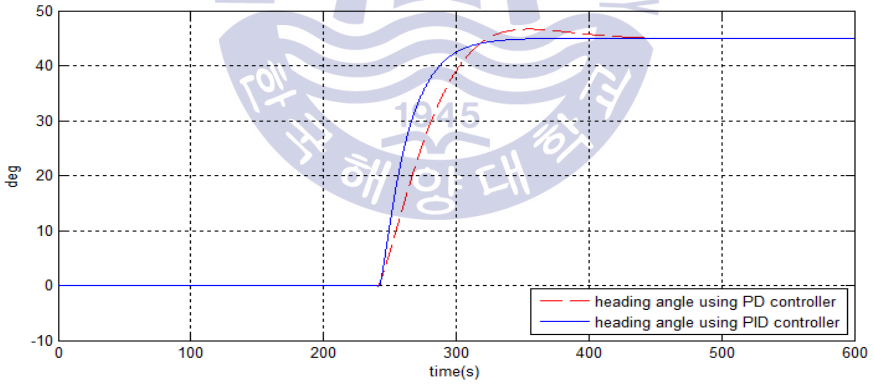

Fig. 3.9 Comparison of heading angles using PD and fuzzy PID autopilot

(3) When the course change angle 60[deg]

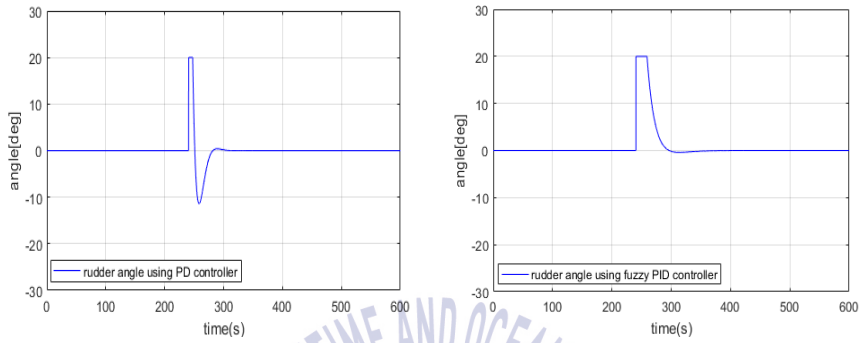

Fig. 3.10 Comparison of rudder angles using PD and fuzzy PID autopilot

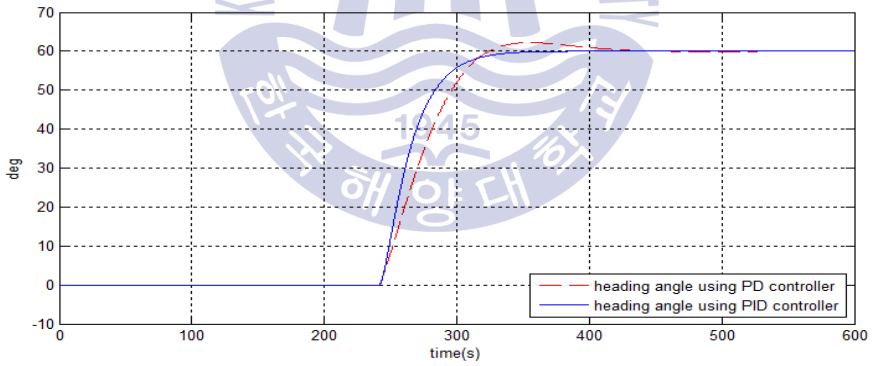

Fig. 3.11 Comparison of heading angles using PD and fuzzy PID autopilot

Fig. 3.6, Fig. 3.8 and Fig. 3.10 are simulation results comparing the rudder angle of the PD type autopilot with that of the fuzzy PID type autopilot when the course change angles are 30°, 45° and 60°. As shown in the simulation results are occurred, the larger the rudder angle is, the bigger overshoot are occurred and the more deviation appears from the route for the PD type autopilot. However, since the fuzzy PID autopilot does not cause overshoot and the rudder angle is changed smoothly, the energy loss of the ship may be smaller than that of the PD autopilot.

Fig. 3.7, Fig. 3.9 and Fig. 3.11 show the simulations comparing the heading angles of PD type autopilot with fuzzy PID autopilot. Since the ship model used in the simulations is liner, both autopilots have no steady-state errors, but the PD autopilot has lower performance in view of response speed, overshoot, and settling time than fuzzy PID autopilot. As the result of the above simulations, the performance of the fuzzy PID autopilot system is verified.

In this paper, velocity type fuzzy PID autopilot system is basically applied.

3.2.2 Path following simulation(velocity type fuzzy PID autopilot)

The simulation conditions are the same as in 2.5.1, and the velocity type fuzzy PID autopilot system is used instead of PD autopilot system in order to prove the path following ability. Here, it is assumed that there are no unknown disturbances like wave, wind and current.

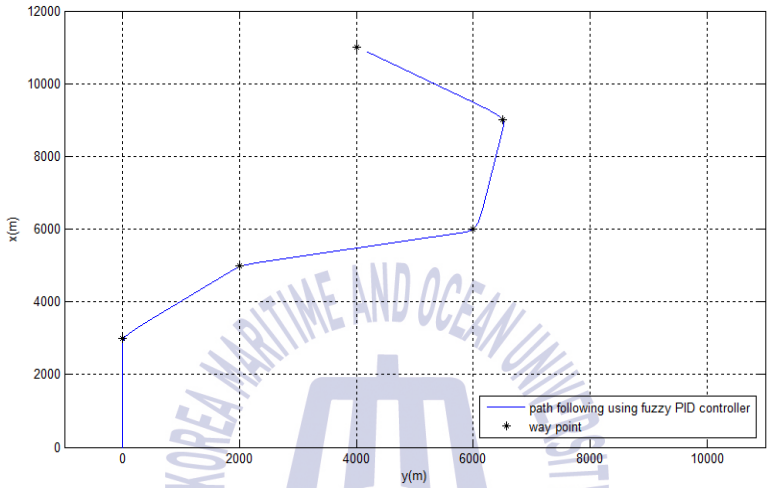

Fig. 3.12 Path following using fuzzy PID autopilot

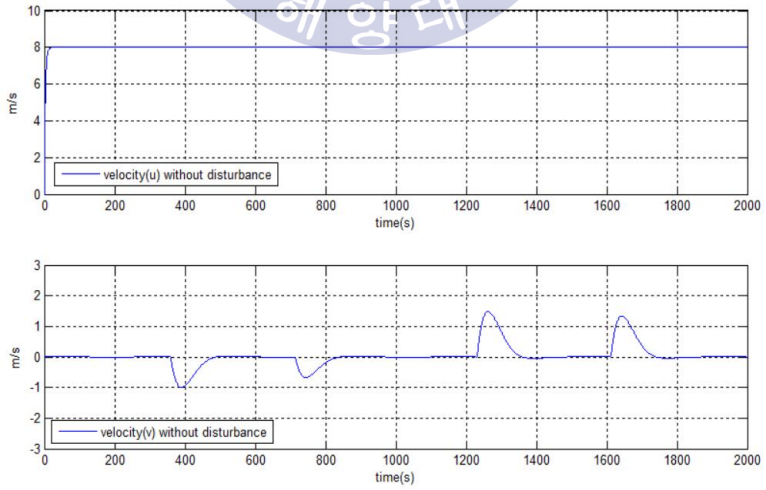

Fig. 3.13 Velocity u and v using fuzzy PID autopilot

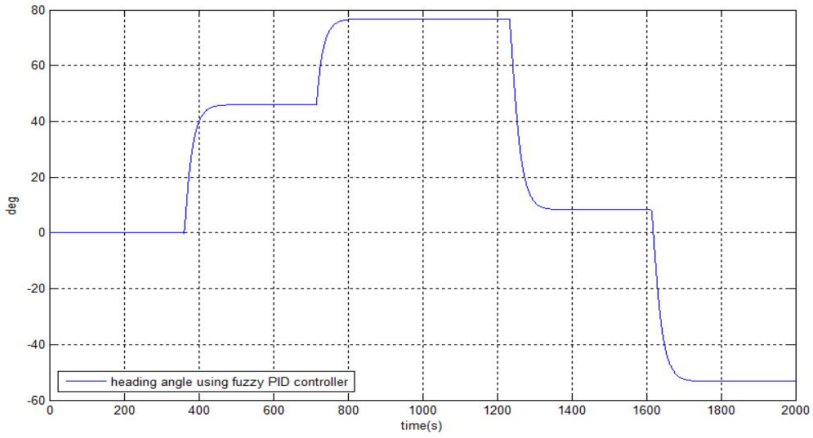

Fig. 3.14 Heading angle using fuzzy PID autopilot

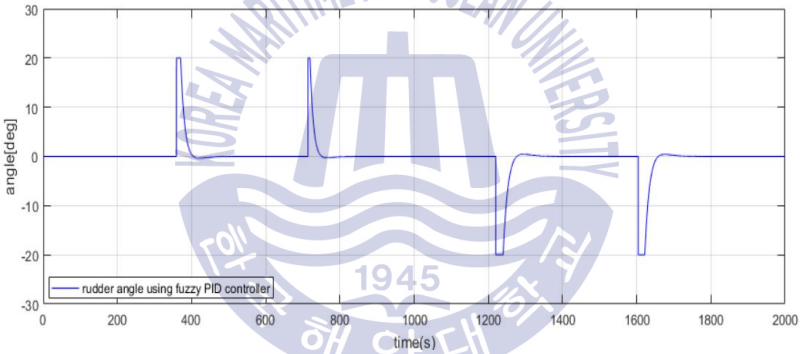

Fig. 3.15 Rudder angle using fuzzy PID autopilot

As shown in the above four simulations, it can be confirmed that the performance of the velocity type fuzzy PID autopilot system is better than that of PD type autopilot system discussed in 2.6.2.

Until now, it was assumed that the ship motion is not affected by environmental disturbances such as current, wave and wind. However, in real maneuvering of the ship, external forces by current, wave, wind and etc. are applied to the ship. Therefore, in chapter 4, the models of current, wave, and wind are combined with the equation of ship motion deal with the actual ship motion.

Chapter 4 Environmental disturbances

In the motion of the ship, if the current, wave, wind are not applied outside of the ship, the ship may not deviate from the designated route and it can be moved economically. However, in an actual navigation circumstance, such environmental disturbances can not be avoided. Therefore, in chapter 4, three types of model for wind, wave and current to generate environmental disturbances very similar to the real environment. These models are combined with the equation of ship motion to make the actual navigation environment.

4.1 Current

4.1.1 Current generation model

Current generation model is approximated as a first-order Gauss-Markov process and the average current speed $V_c(t)$ is modeled as the differential equation given as Equation (4.1) [5].

$$\dot{V}_c(t)+\mu_0 V_c(t)=w(t) \tag{4.1}$$

Here, $w(t)$ means a white gaussian noise with a zero mean , where μ_0 has

a value equal to or greater than 0 but typically selected as 0. To make the average speed of current similar to the real environment, it is necessary to set the range of the average current speed as $V_{\min} \le V_c(t) \le V_{\max}$ and the following algorithm generates a current speed.

1). Set initial value $V_c(0) = 0.5(V_{\max} + V_{\min})$

2). Execute Euler integration with sampling time h

$$\dot{V}_c = \frac{V_c(k+1) - V_c(k)}{h} = w(k)$$

3). Limit $\mathrm{if}(V_c(k+1) > V_{\max})$ or $(V_c(k+1) < V_{\max})$,

$$V_c(k+1) = V_c(k) + hw(k)$$

4). Let $k = k+1$, and then return to step 2).

Here, h is sampling time, $V_{\min}$ and $V_{\max}$ are the minium and maximum value of the current speed.

4.1.2 Current generation simulations

(1) In case of current maximum speed 5m/s, minium speed 3m/s and average speed 4m/s

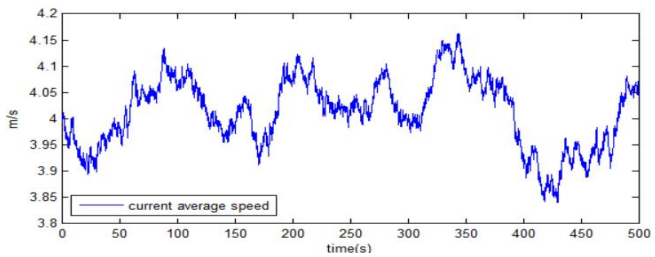

Fig. 4.1 The generated current speed model

(2) In case of current maximum speed 2m/s, minium speed 0m/s and average speed 1m/s

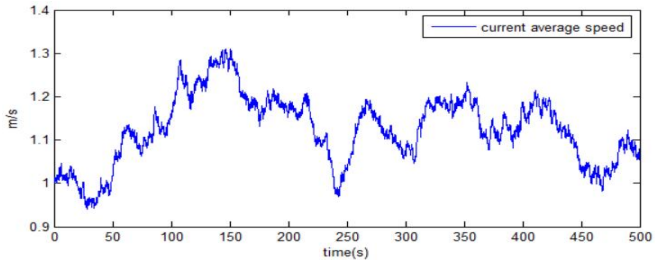

Fig. 4.2 The generated current speed model

4.1.2 Effect of current on the ship

In the earth fixed coordinate system, the two dimensional current is represented as Fig. 4.3 with average current speed V_c and current direction β.

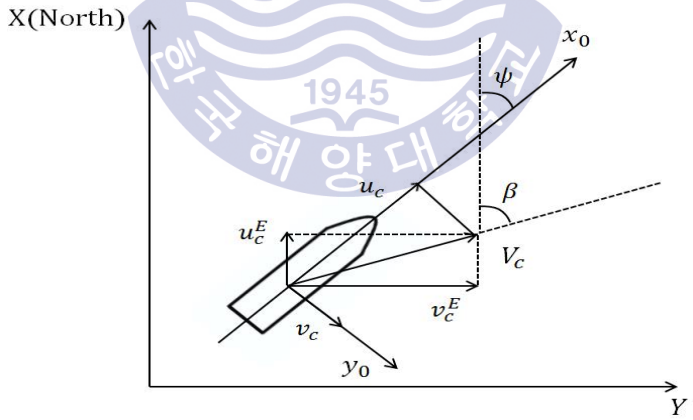

Fig. 4.3 Definition of average velocity V_c and direction β of the current for a ship

The two-dimensional current speed for the ship in the earth fixed coordinate system is described by Equation (4.2), where u_c^E and v_c^E are current velocity components in X and Y direction of the earth-fixed coordinate system.

$$u_c^E = V_c \cos\beta$$
$$v_c^E = V_c \sin\beta \tag{4.2}$$

However, since the average speed of current acting on the ship must be represented based on the body-fixed coordinate system, it is necessary to convert the two dimensional current speed of the earth-fixed coordinate system to that of the body-fixed coordinate system. Therefore, the resultant conversion equations are given in Equation (4.3) as function of angle β and heading angle ψ.

$$u_c = V_c \cos(\beta - \psi)$$
$$v_c = V_c \sin(\beta - \psi) \tag{4.3}$$

4.2 Wind

4.2.1 Wind generation model

The mathematical model to generated wind is given by Equation (4.4).

$$\dot{x}_1 = w_2$$
$$\dot{x}_2 = -\frac{1}{D}(x_2 - Kw_3) \tag{4.4}$$
$$V_R = x_1 + x_2$$

Here, w_2 and w_3 mean white gaussian noises with zero mean, K is constant

value for time, D is constant value for gain, where K and D consist of $K = \sqrt{5286 k V_R(10)}$, $D = \sqrt{286 / V_R(10)}$. $V_R(10)$ is the speed of the wind above the basis of sea level and it is assumed that k has the value of 0.05 as turbulence factor.

4.2.2 Effect of wind on ship

(1) Definition of wind speed V_R and wind direction γ_R

The following Fig. 4.4 is to define wind speed V_R and wind direction γ_R on the earth-fixed and body-fixed coordinate system.

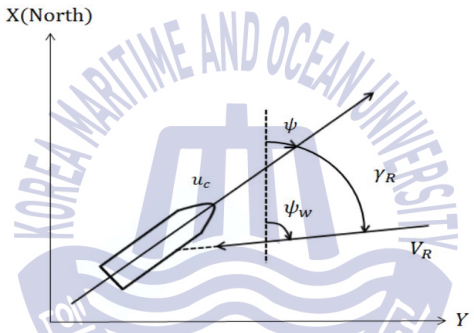

Fig. 4.4 Definition of velocity V_R and direction γ_R of the wind for a ship

(2) Wind forces and moments

The forces and moments of the wind are represented by the following force vector.

$$\tau_{wind} = [X_{wind}, Y_{wind}, N_{wind}]^T \tag{4.5}$$

Here, X_{wind}, Y_{wind} and N_{wind} are the forces and moments of the wind. τ_{wind} is a part of $\tau_{disturbance}$ in Equation (2.1) and acts as an element to interfere with ship motion. Wind forces and moments X_{wind}, Y_{wind} and N_{wind} are suggested by Isherwood like Equation (4.6) [18].

$$X_{wind} = \frac{1}{2} C_X(\gamma_R) \rho_w V_R^2 A_T$$

$$Y_{wind} = \frac{1}{2} C_Y(\gamma_R) \rho_w V_R^2 A_L \tag{4.6}$$

$$N_{wind} = \frac{1}{2} C_N(\gamma_R) \rho_w V_R^2 A_L L$$

Here, C_X and C_Y are the force coefficients, C_N is moment coefficient, and ρ_w is the density of air. C_X, C_Y and C_N are equivalent to Equation (4.7).

$$C_X = A_0 + A_1 \frac{2A_L}{L^2} + A_2 \frac{2A_T}{B^2} + A_3 \frac{L}{B} + A_4 \frac{S}{L} + A_5 \frac{C}{L} + A_6 M$$

$$C_Y = B_0 + B_1 \frac{2A_L}{L^2} + B_2 \frac{2A_T}{B^2} + B_3 \frac{L}{B} + B_4 \frac{S}{L} + B_5 \frac{C}{L} + B_6 \frac{A_{SS}}{A_L} \tag{4.7}$$

$$C_N = C_0 + C_1 \frac{2A_L}{L^2} + C_2 \frac{2A_T}{B^2} + C_3 \frac{L}{B} + C_4 \frac{S}{L} + C_5 \frac{C}{L}$$

Here, $L, B, A_L, A_T, A_{SS}, S, C$ and M are shown in Table. 4.1. $A_i, B_i (i = 0...6)$, and $C_j (j = 0...5)$ are shown in Table. 4.2 to Table. 4.4.

Table 4.1 Definition of $L, B, A_L, A_T, A_{SS}, S, C$ and M

L	length overall
B	beam
A_L	lateral projected area
A_T	transverse projected area
A_{SS}	lateral projected area of superstructure
S	length of perimeter of lateral projection of model
C	distance from bow of centroid of lateral projected area
M	number of distinct groups of masts or kingposts seen in lateral projection

Table 4.2 Surge induced wind force parameters (Isherwood 1972)

γ_R(deg)	A_0	A_1	A_2	A_3	A_4	A_5	A_6	S.E
0	2.152	-0.500	0.243	-0.164				0.086
10	1.714	-3.33	0.145	-0.121				0.104
20	1.818	-3.97	0.244	-0.143			0.033	0.096
30	1.965	-4.81	0.243	-0.154			0.041	0.117
40	2.333	-5.99	0.247	-0.190			0.042	0.115
50	1.726	-6.54	0.189	-0.173	0.348		0.048	0.109
60	0.913	-4.68		-0.104	0.482		0.052	0.082
70	0.454	-2.88		-0.068	0.346		0.043	0.077
80	0.341	-0.91		-0.089			0.032	0.090
90	0.355				-0.247		0.018	0.094
100	0.601				-0.372		-0.020	0.096
110	0.651	1.29			-0.582		-0.031	0.090
120	0.564	2.54			-0.748		-0.024	0.100
130	-0.142	3.58		0.047	-0.700		-0.028	0.105
140	-0.677	3.64		0.069	-0.529		-0.032	0.123
150	-0.723	3.14		0.064	-0.475		-0.032	0.128
160	-2.148	2.56		0.081		1.27	-0.027	0.123
170	-2.707	2.97	-0.175	0.126		1.81		0.115
180	-2.529	3.76	-0.174	0.128		1.55		0.112

Table 4.3 Sway induced wind force parameters (Isherwood 1972)

γ_R(deg)	B_0	B_1	B_2	B_3	B_4	B_5	B_6	S.E
10	0.096	0.22						0.015
20	0.176	0.71						0.023
30	0.225	1.38		0.023		-0.29		0.030
40	0.329	1.82		0.043		-0.59		0.054
50	1.164	1.26	0.121		-0.242	-0.95		0.055
60	1.163	0.96	0.101		-0.177	-0.88		0.049
70	0.916	0.53	0.069			-0.65		0.047
80	0.844	0.55	0.082			-0.54		0.046
90	0.889		0.138			-0.66		0.051
100	0.799		0.155			-0.55		0.050
110	0.797		0.151			-0.55		0.049
120	0.996		0.184		-0.212	-0.66	0.34	0.047
130	1.014		0.191		-0.280	-0.69	0.44	0.051
140	0.784		0.166		-0.209	-0.53	0.38	0.060
150	0.536		0.176	-0.029	-0.163		0.27	0.055
160	0.251		0.106	-0.022				0.036
170	0.125		0.046	-0.012				0.022

Table 4.4 Yaw induced wind moment parameters (Isherwood 1972)

γ_R(deg)	C_0	C_1	C_2	C_3	C_4	C_5	S.E
10	0.0596	0.061				-0.074	0.0048
20	0.1106	0.204				0.170	0.0074
30	0.2258	0.245				-0.380	0.0105
40	0.2017	0.457		0.0067		-0.472	0.0137
50	0.1759	0.573		0.0118		-0.523	0.0149
60	0.1925	0.480		0.0115		-0.546	0.0133
70	0.2133	0.315		0.0081		-0.526	0.0125
80	0.1827	0.254		0.0053		-0.443	0.0123
90	0.2627					-0.508	0.0141
100	0.2102		-0.0195		0.0335	-0.492	0.0146
110	0.1567		-0.0258		0.0497	-0.457	0.0163
120	0.0801		-0.0311		0.0740	-0.396	0.0179
130	-0.0189		-0.0488	0.0101	0.1125	-0.420	0.0166
140	0.0256		-0.0422	0.0100	0.0889	-0.463	0.0162
150	0.0552		-0.0381	0.0109	0.0689	-0.476	0.0141
160	0.0881		-0.0306	0.0091	0.0366	-0.415	0.0105
170	0.0851		-0.0122	0.0025		-0.220	0.0057

4.3 Wave

4.3.1 Wave generation model

Since the state space equation for generating wave can be made using the PM(Pierson-Moskowitz) spectrum, the PM spectrum is described. Pierson and Moskowitz developed a spectrum of wind-induced wave and PM spectrum $S(\omega)$ is written as Equation (4.8) [4].

$$S(\omega) = J\omega^{-5}\exp(-K\omega^{-4})\,(m^2/s) \tag{4.8}$$

Here, J and K are defined by Equation (4.9).

$$J = 8.1\times10^{-3}g^2,\ K = 0.74\left(\frac{g}{V}\right)^4 \tag{4.9}$$

Here, g is the gravity constant and V is the wind speed. Then, the wave

height H_s and the frequency ω_0 of the wave are given by Equation (4.10).

$$H_s = 0.21\frac{V^2}{g},\ \omega_0 = 0.88\frac{g}{V} \tag{4.10}$$

The power spectral density function $P_{yy}(\omega)$, which is a linearly approximated as means for expressing $S(\omega)$ to a state space equation, is an output $y(s)$ when $w(s)$ is input. And $y(s)$ consists of Equation (4.11).

$$y(s) = h(s)w(s) \tag{4.11}$$

Here, $h(s)$ means transfer function and $w(s)$ means a normalized white gaussian noise with a zero mean. Therefore, the linearized power spectral density function $P_{yy}(\omega)$ is written as Equation (4.12).

$$P_{yy}(\omega) = |h(j\omega)|^2 \tag{4.12}$$

And for this spectral density function, transfer function $h(s)$ is assumed to be Equation (4.13).

$$h(s) = \frac{K_w s}{s^2 + 2\lambda\omega_0 s + \omega_0^2} \tag{4.13}$$

The gain K_w is $2\lambda\omega_0\sigma_w$, where σ_w is density of wave, λ is damping coefficient and ω_0 is frequency of wave. In order to obtain σ_w, the transfer function of Equation (4.13) is transformed into the frequency domain expression as shown in Equation (4.14).

$$h(j\omega) = \frac{j2(\lambda\omega_0\sigma_w)\omega}{(\omega_0^2 - \omega^2) + j2\lambda\omega_0\omega}$$

$$|h(j\omega)| = \frac{2(\lambda\omega_0\sigma_w)\omega}{\sqrt{(\omega_0^2 - \omega^2)^2 + 4(\lambda\omega_0\omega)^2}} \tag{4.14}$$

$$P_{yy}(\omega) = |h(j\omega)|^2 = \frac{4(\lambda\omega_0\sigma_w)^2\omega^2}{(\omega_0^2 - \omega^2)^2 + 4(\lambda\omega_0\omega)^2}$$

The maximum value of the power spectral density $P_{yy}(\omega)$ can be obtained in case of $\omega = \omega_0$, and it is possible to obtain the σ_w. This can be expressed as Equation (4.15). Based on σ_w, the linearly approximated state space equation for the wave is given by Equation (4.16).

$$\max P_{yy}(\omega)|_{\omega=\omega_0} = \sigma_w^2 \tag{4.15}$$

$$\begin{bmatrix} \dot{\psi}_H \\ \dot{\xi}_H \end{bmatrix} = \begin{bmatrix} -\omega_0^2 - 2\lambda\omega_0 \\ 0 \quad 1 \end{bmatrix} \begin{bmatrix} \psi_H \\ \xi_H \end{bmatrix} + \begin{bmatrix} K_w \\ 0 \end{bmatrix} w_1$$
$$y = [1 \;\; 0] \begin{bmatrix} \psi_H \\ \xi_H \end{bmatrix} \tag{4.16}$$

Here, w_1 means a white gaussian noise with zero mean and variance of 1.

4.3.2 Wave generation simulations

(1) In case that wind speed is 10m/s and wave frequency is 0.3[rad/s]

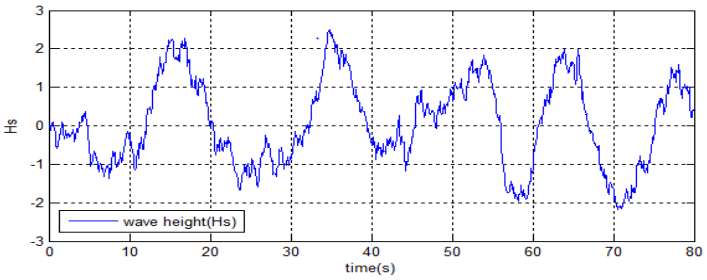

Fig. 4.5 The generated wave model

If the wind speed is $10m/s$, the wave height should be $2.15m$ according to Equation (4.10). Simulation result shows that it is similar to $2.15m$. since the frequency of the wave is $0.3rad/s$, about 21 second period should come out. This is also similar to 21 seconds according to simulation.

(2) In case that wind speed is 5m/s and wave frequency is 0.45[rad/s]

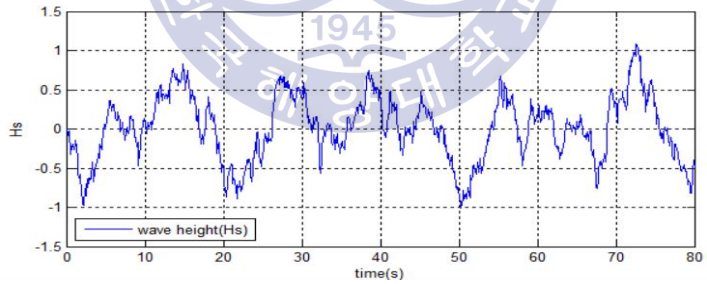

Fig. 4.6 The generated wave model

If the wind speed is $5m/s$, the wave height should be $0.45m$ according to Equation (4.10). Simulation result shows that it is similar to $0.45m$. And about 15 seconds period should come out according to simulation.

4.3.2 Effect of wave on ship

When the frequency w_0 of the wave is applied to the ship, the actual frequency of the wave affecting the ship, which changes according to the heading angle, is expressed by Equation (4.17).

$$\omega_e(U,\omega_0,\alpha) = \omega_0 - \frac{\omega_0^2}{g} U\cos\alpha \tag{4.17}$$

Here, ω_e is the frequency of the actual wave applied to the ship. U is ship forward direction speed, and α is the angle between heading angle and wave direction. α is defined in Fig. 4.7.

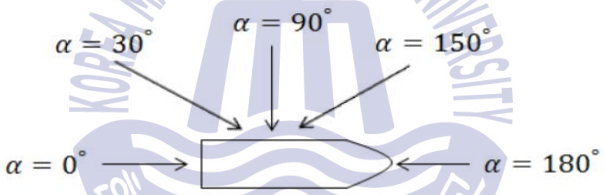

Fig. 4.7 Angle between heading angle and wave direction

4.4 3 DOF ship equation of motion combined with current, wind and wave model

So far, to create a realistic environment, current, wind, and wave model and how to create the them were surveyed. In section 4.4, three environmental disturbance models are combined into the 3 DOF ship equation of motion. Equation (4.18) is a 3 DOF state equation of a ship combined with three environmental disturbances.

$$\dot{x} = Ax + Bu + \tau_{disturbance}$$

$$A = \begin{bmatrix} 0 & 0 & 0 & \cos\psi & -\sin\psi & 0 \\ 0 & 0 & 0 & \sin\psi & \cos\psi & 0 \\ 0 & 0 & 0 & 0 & 0 & 1 \\ 0 & 0 & 0 & c & 0 & 0 \\ 0 & 0 & 0 & 0 & a_{11} & a_{12} \\ 0 & 0 & 0 & 0 & a_{21} & a_{22} \end{bmatrix}, B = \begin{bmatrix} 0 & 0 \\ 0 & 0 \\ 0 & 0 \\ d & 0 \\ 0 & b_1 \\ 0 & b_2 \end{bmatrix} \tag{4.18}$$

$$\tau_{disturbance} = \begin{bmatrix} 0 \\ 0 \\ 0 \\ -c\cos(\beta-\psi-\psi_H)V_c + X_{wind} \\ -a_{11}\sin(\beta-\psi-\psi_H)V_c + Y_{wind} \\ -a_{21}\sin(\beta-\psi-\psi_H)V_c + N_{wind} \end{bmatrix}$$

Here, state vector x is $[x, y, \psi, u, v, r]^T$ and u is $[T, \delta]^T$. $\tau_{disturbance}$ is a force and moment added to the ship by current, wind, and wave, which directly affect the speed and angular velocity of the ship and act as an obstacle to the movement of the ship. And ψ_H means the vibration motion of the wave.

4.5 Simulation of ship motion under disturbances

4.5.1 Simulation condition 1

The specifications of the ship are shown in Table 2.3 and the ship model is used by discretizing Equation (4.17) by Euler method. And the conditions of environmental disturbances are shown in Table 4.5.

Table 4.5 Conditions of environmental disturbances

Environmental condition	
current direction(deg)	-80
current average speed(m/s)	1.2
wave direction(deg)	30
wave period(s)	5.23
wave amplitude(m)	0.26
wind speed$(knot)$	10
wind direction(deg)	30

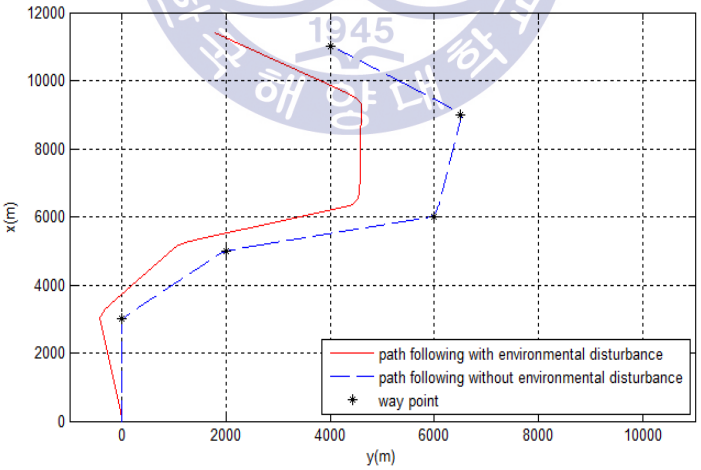

Fig. 4.8 Comparison of path following with and without environmental disturbances

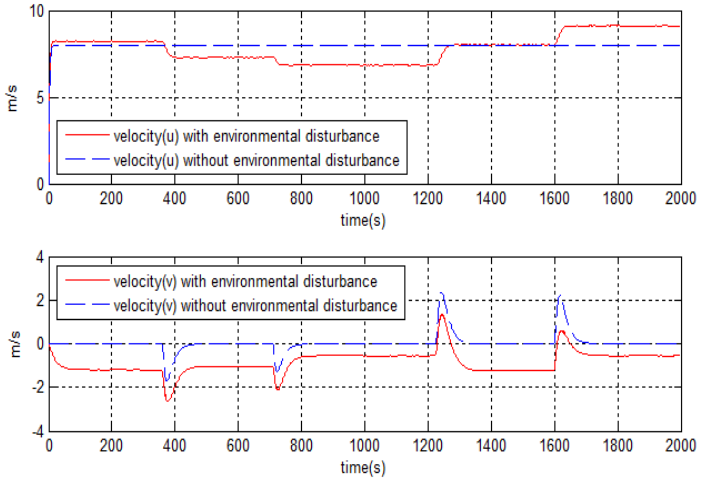

Fig. 4.9 Comparison of velocities with and without environmental disturbances

Fig. 4.8 and Fig. 4.9 show the comparison of simulation results between the case that the environmental disturbances are applied to the ship and the case that the environmental disturbances are not applied. Fig. 4.8 shows the movement of the ship. In case the environmental disturbances are not applied to the ship, the ship can maintain the designated route without great deviation. But in case the environmental disturbances are applied to the ship, the ship can not maintain the route and deviates from the route. Fig. 4.9 shows the comparison of the speed of the ship. In case the environmental disturbances are not applied to the ship, the forward direction speed of the ship is maintained as the initial set value $8m/s$, and the lateral speed also does not appear in the range except the course change. But in case the environmental disturbances are applied to the ship, the forward direction speed of the ship is not maintained as the initial set value $8m/s$, and the lateral speed also appears even in the range except the course change. Since the lateral speed component is occurred, the ship can not maintain the designated route.

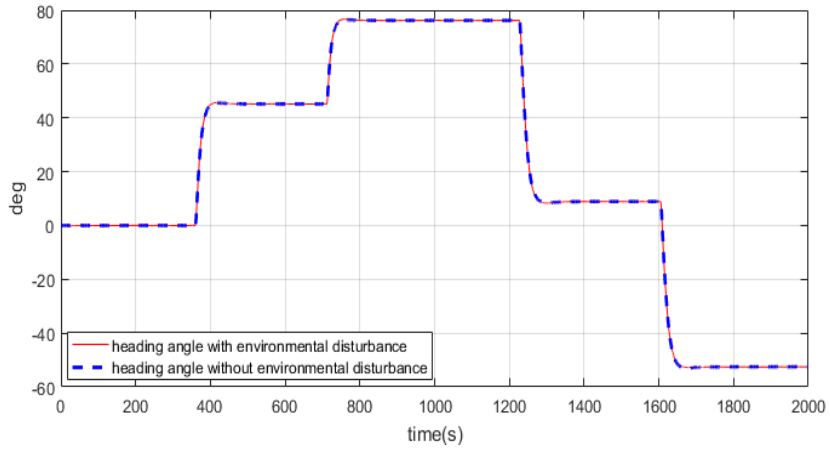

Fig. 4.10 Comparison of heading angles with and without environmental disturbances

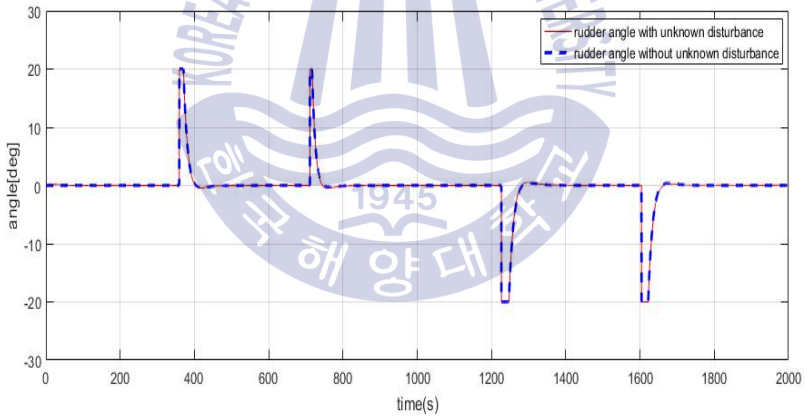

Fig. 4.11 Comparison of rudder angles with and without environmental disturbances

Fig. 4.10 is the simulation result of the ship heading angle. Due to the autopilot system, it can be seen that even if environmental disturbances are applied to a ship, the ship can maintain the reference heading angle. Fig. 4.11 is the simulation result of the ship rudder angle. In order to assure the stability of the ship, the rudder angle is limited to $\pm 20^{\circ}$.

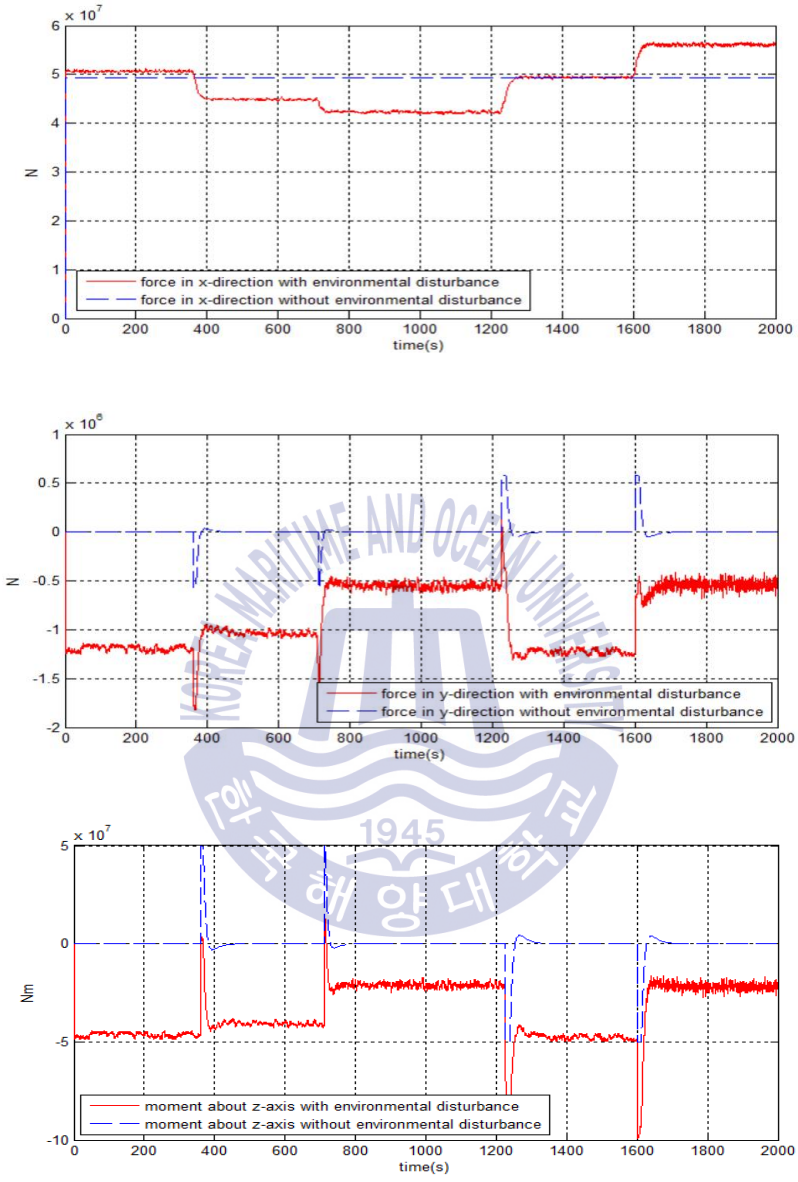

Fig. 4.12 Comparison of forces and moments with and without environmental disturbances

As shown in Fig. 4.8 and Fig. 4.9, in case the environmental disturbances are applied to the ship, the forward direction and lateral speed are generated because the additional forces and moments by disturbances are applied to the ship. The first figure in Fig. 4.12 is a simulation result comparing the forces in the x-axis direction of the ship when the environmental disturbances are applied to the ship with the force when they are not. When the environmental disturbances are applied to the ship, it can be seen that the changing forces are added to the ship according to the change of the reference heading angle. The second and third figures in Fig. 4.12 show the forces and moments acted on the ship during performing steering motion. It is also known that there are additional forces and moments due to environmental disturbances.

4.5.2 Simulation condition 2

The ship model and the its specifications are the same as in 4.5.1, and the simulation was performed under different conditions of environmental disturbances. The conditions of the environmental disturbances are shown in Table. 4.6.

Table 4.6 Conditions of environmental disturbances

Environmental conditions	
current direction(deg)	30
current average speed(m/s)	0.8
wave direction(deg)	60
wave period(s)	0.85
wave amplitude(m)	0.14
wind speed($knot$)	5
wind direction(deg)	60

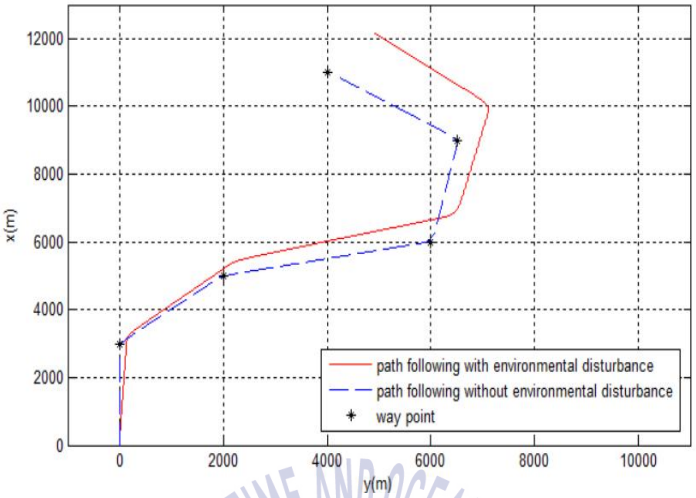

Fig. 4.13 Comparison of path following with and without environmental disturbances

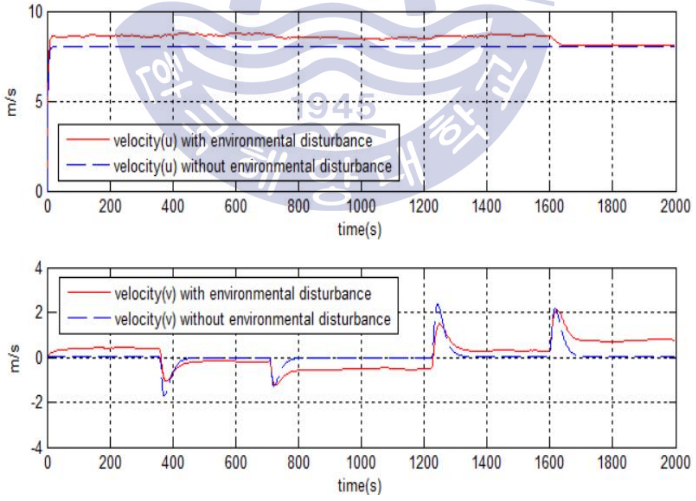

Fig. 4.14 Comparison of velocities with and without environmental disturbances

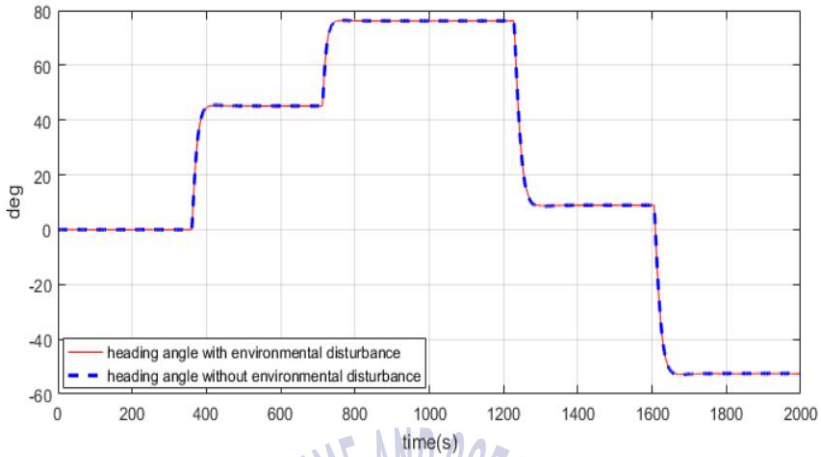

Fig. 4.15 Comparison of heading angles with and without environmental disturbances

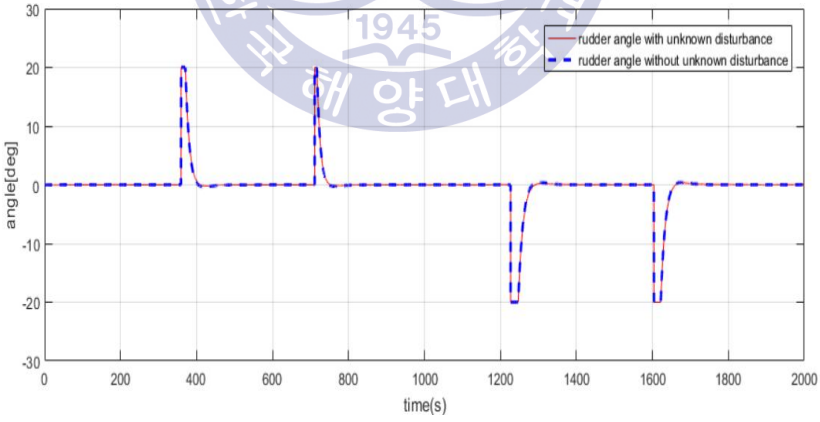

Fig. 4.16 Comparison of rudder angles with and without environmental disturbances

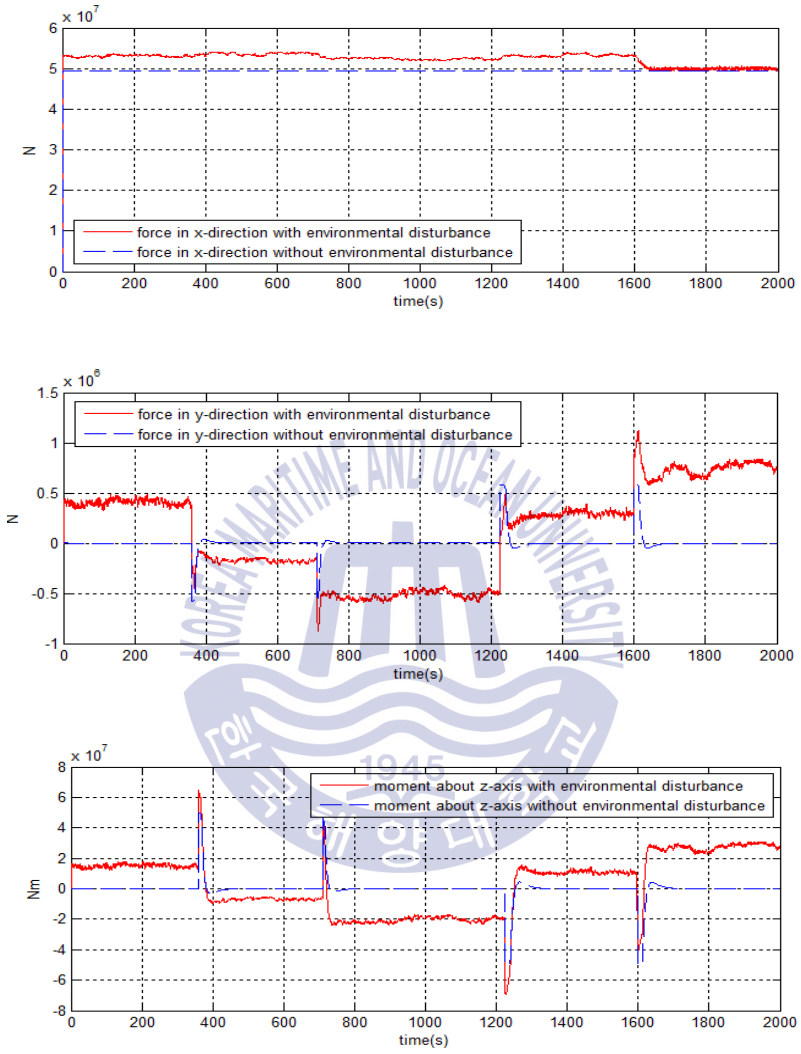

Fig. 4.17 Comparison of forces and moments with and without environmental disturbances

Because the explanation of the simulation condition 2 is very similar to the simulation condition 1, the explanation of the simulation results is omitted.

When environmental disturbances are applied to the ship, additional forces and moments are applied to the ship, so that the forward direction speed u and lateral speed v are changed depending on the change of the reference heading angle, and the ship deviates from the designated route. In order to solve such problems, in chapter 5, a heading angle keeping control system that uses the separation principle is suggested, based on a ship linear discrete stochastic model that includes white Gaussian noises and environmental disturbances.

Chapter 5 Velocity type fuzzy PID autopilot system using separation principle based on Kalman filter

5.1 Linear discrete stochastic state space model of ship including white Gaussian noise

$$x_k = Ax_{k-1} + Bu_{k-1} + Dw_{k-1}$$

$$A' = \begin{bmatrix} 0\,0\,0 & \cos\psi & -\sin\psi & 0 \\ 0\,0\,0 & \sin\psi & \cos\psi & 0 \\ 0\,0\,0 & 0 & 0 & 1 \\ 0\,0\,0 & c & 0 & 0 \\ 0\,0\,0 & 0 & a_{11} & a_{12} \\ 0\,0\,0 & 0 & a_{21} & a_{22} \end{bmatrix}, B' = \begin{bmatrix} 0 & 0 \\ 0 & 0 \\ 0 & 0 \\ c & 0 \\ 0 & d_1 \\ 0 & d_2 \end{bmatrix}, D' = \begin{bmatrix} 0 \\ 0 \\ 0 \\ 1 \\ 1 \\ 1 \end{bmatrix} \tag{5.1}$$

$$A, B, D = discrete\, A', B', D' using\ Euler discretization$$

$$z_k = Cx_k + v_k,\ C = I_{6\times 6}, v_k = \begin{bmatrix} v_{k1_{3\times 1}} \\ v_{k2_{3\times 1}} \end{bmatrix} \tag{5.2}$$

Equation (5.1) is a discrete stochastic state equation with system noise, where the system noise w_{k-1} is assumed to be a white gaussian noise with a zero mean. And Equation (5.2) is the output equation of the discrete

stochastic system including the measurement noise. Here, v_{k1} is the measurement noise contained during measuring the position and heading angle of the ship with GPS and gyro compass, and v_{k2} is the measurement noise contained when the ship speed and angular velocity are measured. These models are used to comprise Kalman filter in order to estimate unknown disturbances using the characteristic of innovation process. v_{k1} and v_{k2} are also assumed to be white gaussian noises with zero mean.

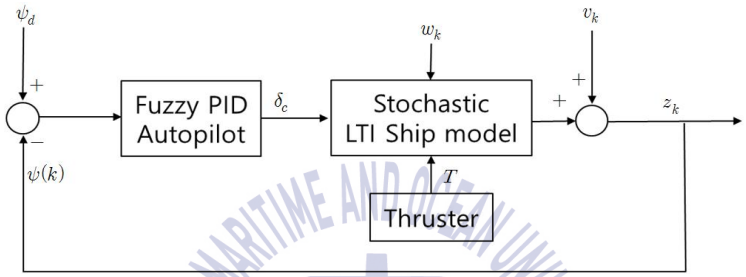

Fig. 5.1 Fuzzy PID autopilot system

Fig. 5.1 is an autopilot system based on fuzzy PID control using $\psi(k)$ with the measurement noise contained during measuring heading angle by gyro compass. Fig. 5.2 and Fig. 5.3 show the simulation results to see how the autopilot system is influenced by the noise.

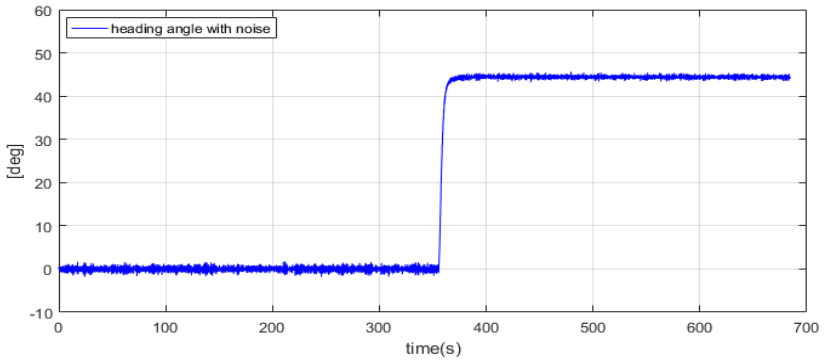

Fig. 5.2 Heading angle with measurement noise

Fig. 5.2 is the simulation result that shows the heading angle of the ship contained measurement noise. It can be seen that the heading angle of the ship does not show a good response due to the influence of noise.

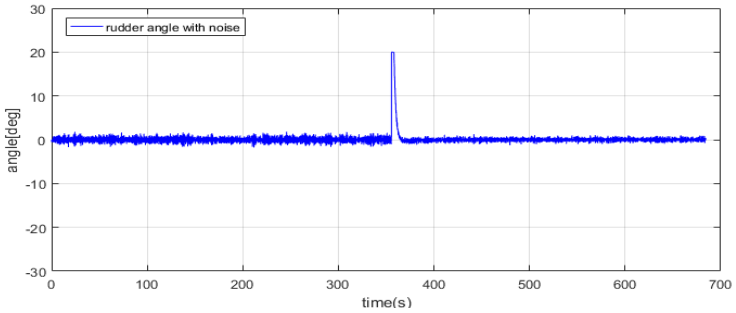

Fig. 5.3 Rudder angle with measurement noise

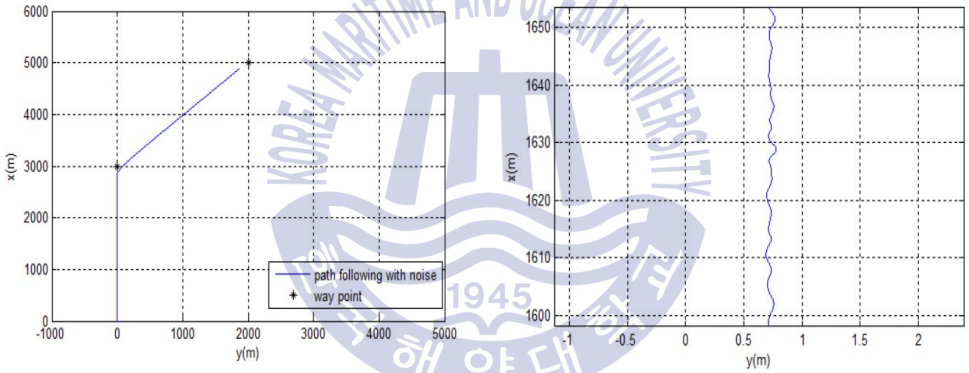

Fig. 5.4 Path following with noise

Fig. 5.3 is the simulation result that shows the rudder angle of the ship subjected to measurement noise when it is measured. When the rudder angle is given under the influence of noise, the ship can not follow designated route accurately as shown in Fig. 5.4. The reason why such poor control performance is occurred is a result of malfunction of the D control by noise influence. Therefore, it is necessary to improve the malfunction of D control due to noise. To do this Kalman filter is introduced to construct a velocity type fuzzy PID autopilot system based on filter state estimation.

5.2 Kalman filter state estimation algorithm in discrete time system

The Kalman filter calculates the filtered estimate of state at the current time, by adding the predicted estimate at the just before sampling time to the compensated estimate which is calculated by multiplying the Kalman weighting matrix by the difference between the real measurement and predicted measurement, called innovation process.

$$\begin{aligned} x_k &= Ax_{k-1} + Bu_{k-1} + Dw_{k-1} \\ z_k &= Cx_k + v_k \end{aligned} \tag{5.3}$$

Equation (5.3) is a discrete time stochastic state space equation with noises. w_{k-1} is a system noise, v_k is a measurement noise, and both w_{k-1} and v_k are assumed to be white gaussian noises with a zero mean. Equation (5.4) is the Kalman filter algorithm.

$$\begin{aligned} \hat{x}_k(-) &= A\hat{x}_{k-1} + Bu_{k-1} \\ P_k(-) &= AP_{k-1}(+)A^T + Q \\ K_k &= P_k(-)C^T\left[CP_k(-)C^T + R_k\right]^{-1} \\ \hat{x}_k &= \hat{x}_k(-) + K_k\left[z_k - C\hat{x}_k(-)\right] \\ P_k &= \left[I - K_kC\right]P_k(-) \end{aligned} \tag{5.4}$$

The initial value of the filter covariance and filter estimate is defined as P_0 and $\hat{x_0}$ At the current sampling time k, the predicted estimate $\hat{x_k}(-)$ and the predicted covariance $P_k(-)$ are calculated according to the first two equations of Equation (5.4). Next, the Kalman gain K_k, which is a weighted matrix, is calculated at the current time k. The filtered estimate value $\hat{x_k}$ is calculated

by adding the predicted estimate value $\hat{x_k}(-)$ by compensated estimate $\triangle\hat{x_k}$. $\triangle\hat{x_k}$ is calculated by multiplying the Kalman gain K_k by the innovation process r_k, where $r_k = z_k - C\hat{x_k}(-)$. This is shown in Equation (5.5).

$$\triangle\hat{x_k} = K_k[z_k - \hat{z_k}(-)] = K_k[z_k - C\hat{x_k}(-)] \tag{5.5}$$

Finally, the filter covariance P_k is calculated to obtain the predicted covariance $P_{k+1}(-)$ at the next sampling time.

5.3 Velocity type fuzzy PID autopilot system based on Kalman filter

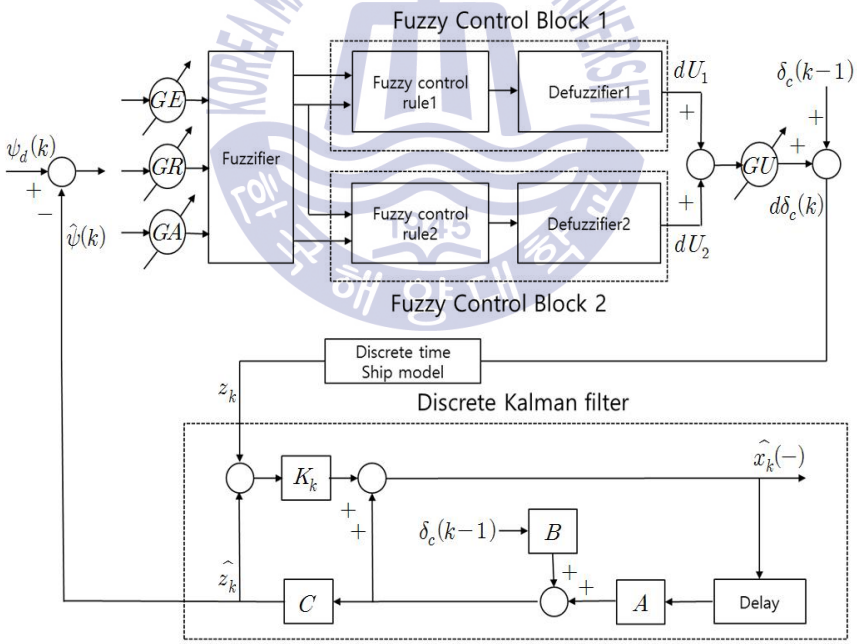

Fig. 5.5 Block diagram of velocity type fuzzy PID autopilot system using separation principle

If the inputs of the velocity type fuzzy PID autopilot using the separation principle are defined again, they are given as Equation (5.6), where $\hat{\psi}(k)$ is filtered estimate of $\psi(k)$ by Kalman filter.

$$\begin{aligned}\psi_e(k) &= \psi_d(k) - \hat{\psi}(k) \\ \psi_r(k) &= [\psi_e(k) - \psi_e(k-1)]/T \\ \psi_a(k) &= [\psi_r(k) - \psi_r(k-1)]/T\end{aligned} \tag{5.6}$$

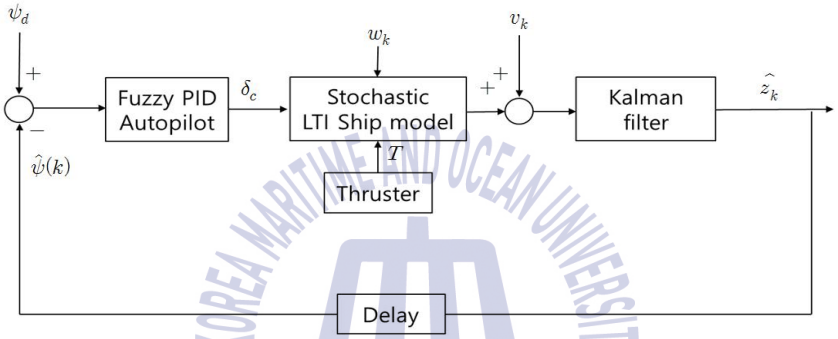

Fig. 5.6 Fuzzy PID autopilot system based on Kalman filter

Fig. 5.6 shows a fuzzy PID autopilot system based on Kalman filter. Since the control is performed using the estimated measurement value $\hat{\psi}(k)$ instead of the actual measurement value $\psi(k)$ which contains the measurement noise, it turns out that the control performance will be improved by reducing the influence of the noise. In order to prove this, simulations are performed using the Equation (5.6) as the inputs of the velocity type fuzzy PID autopilot.

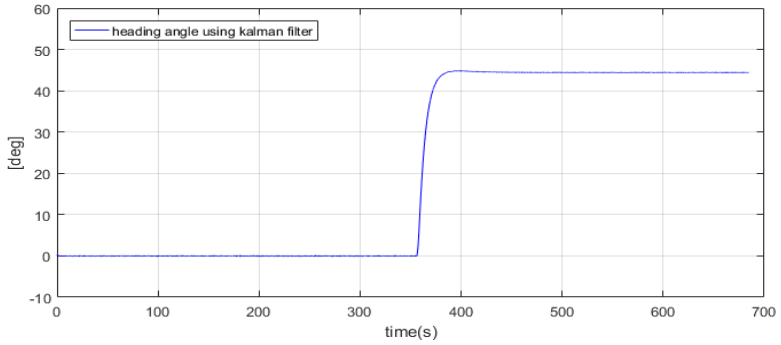

Fig. 5.7 Heading angle using Kalman filter estimate

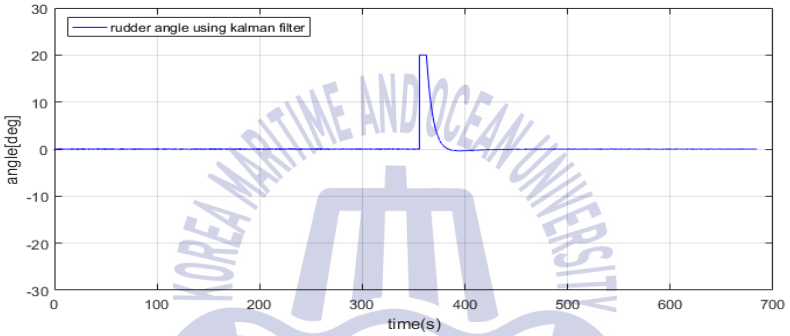

Fig. 5.8 Rudder angle using Kalman filter estimate

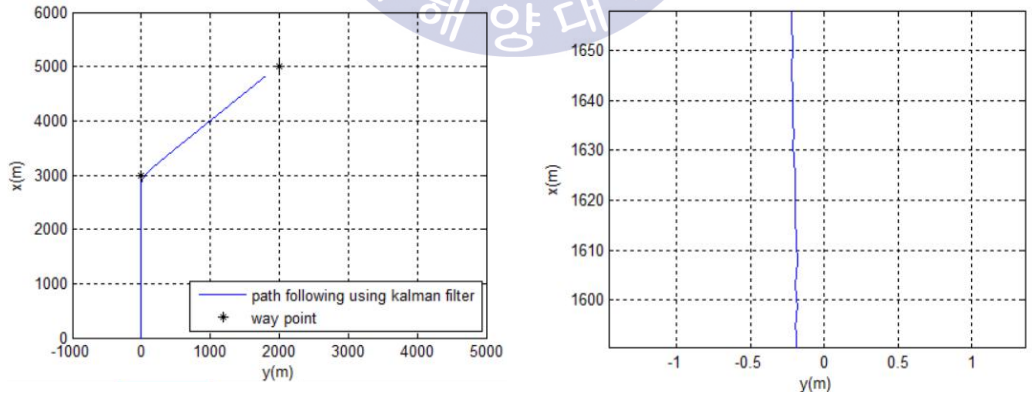

Fig. 5.9 Path following using Kalman filter estimate

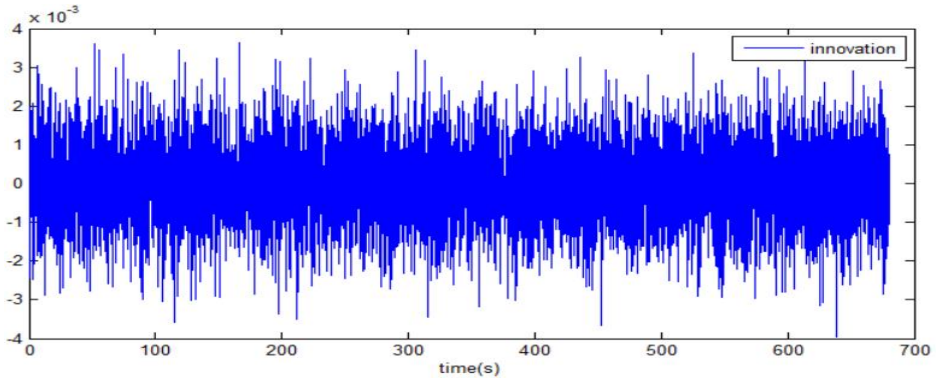

Fig. 5.10 Innovation process of Kalman filter

Fig. 5.7 and Fig. 5.8 show the rudder command angle and heading angle which are controlled by feedback of the estimated output $\hat{\psi}(k)$ by Kalman filter for generating inputs of the fuzzy PID autopilot. Compared the rudder angle of Fig. 5.8 and Fig. 5.2, the influence of noise is remarkably reduced. Fig. 5.9 is the path following simulation result using rudder angle as shown in Fig. 5.8 to control the ship. In contrast to Fig. 5.4, it can be seen that the influence of noise is reduced and good path following is possible. Fig. 5.10 shows the innovation process used to compute filter compensated estimate. Since the expected value of the innovation process converges to zero, it is known that the Kalman filter estimates the heading angle from measured heading statistically well.

5.4 Linear discrete stochastic space state model of ship including unknown disturbances and white Gaussian noises

$$x_k = Ax_{k-1} + Bu_{k-1} + Dw_{k-1} + U_{k-1}$$

$$A' = \begin{bmatrix} 0\,0\,0 & \cos\psi & -\sin\psi & 0 \\ 0\,0\,0 & \sin\psi & \cos\psi & 0 \\ 0\,0\,0 & 0 & 0 & 1 \\ 0\,0\,0 & c & 0 & 0 \\ 0\,0\,0 & 0 & a_{11} & a_{12} \\ 0\,0\,0 & 0 & a_{21} & a_{22} \end{bmatrix}, B' = \begin{bmatrix} 0 & 0 \\ 0 & 0 \\ 0 & 0 \\ c & 0 \\ 0 & d_1 \\ 0 & d_2 \end{bmatrix}, D' = \begin{bmatrix} 0 \\ 0 \\ 0 \\ 1 \\ 1 \\ 1 \end{bmatrix} \tag{5.7}$$

$$U_{k-1}{}' = \begin{bmatrix} 0 \\ 0 \\ 0 \\ -c\cos(\beta-\psi-\psi_H)V_c + X_{wind} \\ -a_{11}\sin(\beta-\psi-\psi_H)V_c + Y_{wind} \\ -a_{21}\sin(\beta-\psi-\psi_H)V_c + N_{wind} \end{bmatrix}$$

$$(A, B, D, U_{k-1}) = (discrete\,A', B', D', U_{k-1}{}')$$

$$z_k = Cx_k + v_k,\ C = I_{6\times 6},\ v_k = \begin{bmatrix} v_{k1_{3\times 1}} \\ v_{k2_{3\times 1}} \end{bmatrix}$$

Equation (5.7) is the linear discrete stochastic state space equation of ship with system noise, measurement noise, and unknown disturbances considered as environmental disturbances. In section 5.4, $\tau_{disturbance}$ is defined as U_{k-1}. To evaluate the performance fuzzy PID autopilot system based on Kalman filter under unknown disturbances, an autopilot system as shown in Fig. 5.11 is considered.

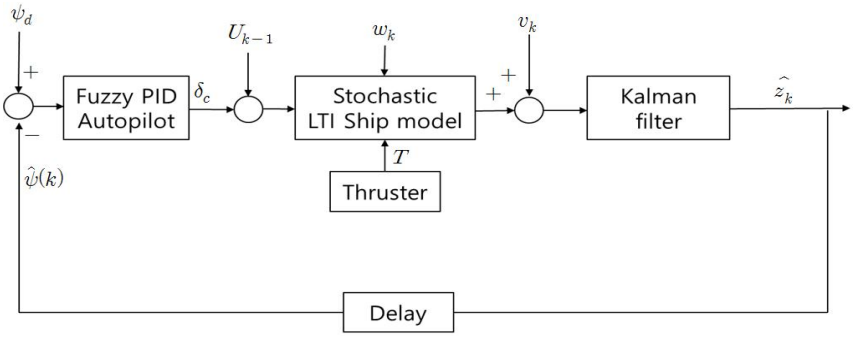

Fig. 5.11 Fuzzy PID autopilot system based on Kalman filter under unknown disturbances

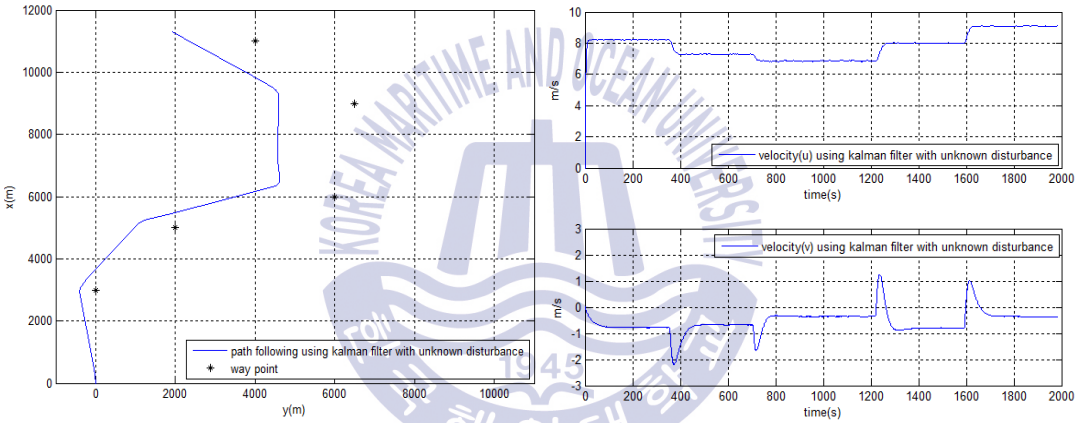

Fig. 5.12 Path following and velocity using Kalman filter under unknown disturbances

The simulation conditions in Fig. 5.11 are the same as those in section 5.3, except that unknown disturbances are added. Fig. 5.12 shows that the ship's speeds are changed due to unknown disturbances. As a result, the reference heading angle is changed and the ship is deviated from the designated route. Since the unknown disturbances alter the ship speed u, v and angular velocity r, the Kalman filter for u, v and r fails to estimate the state, so that the innovation process does not converge to zero, as shown in Fig. 5.13.

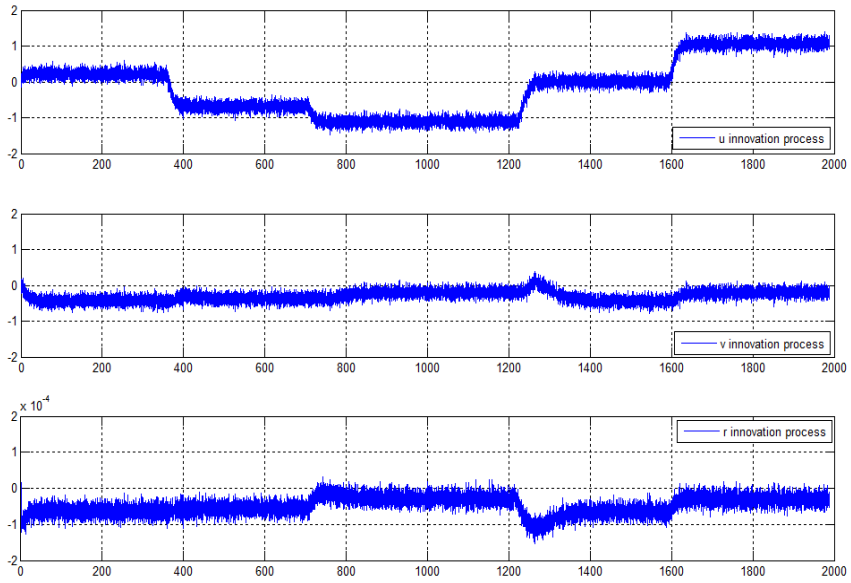

Fig. 5.13 Innovation processes of Kalman filter for u, v and r under unknown disturbances

From simulation results, it is known that if unknown disturbances are applied to the ship, the ship can not maintain the designated route and deviates from the route. In order to solve such a problem, in chapter 6, a fuzzy disturbance estimator is proposed by appropriately using the variation of the innovation process caused by unknown disturbances. The proposed estimator estimates the magnitude of unknown disturbances and the estimated disturbances are feedback to reduce the influence of unknown disturbances.

Chapter 6 Fuzzy disturbance estimator based on the innovation process of Kalman filter

As shown in the simulation results of the previous chapters, the Kalman filter algorithm on the linearized ship model estimates the state of the given system well. However, the Kalman filter can not accurately estimate the motion variables of the ship when unknown disturbances such as current, wave and wind are applied.

In order to compensate for this at first, the existence of an unknown disturbances is determined by using characteristics of the innovation processes that are changed with DC values due to the uncertainty. At second, if existence of unknown disturbances are determined, the fuzzy disturbance estimator estimates the magnitude of the unknown disturbances. At last, the estimated disturbances are feedback to Kalman filter and the output part of the fuzzy PID autopilot in order to reduce the influence of unknown disturbances which interferes with the movement of the ship.

6.1 How to judge the existence of unknown disturbances

Innovation processes that are changed with DC values due to unknown disturbances can not keep statistically zero mean values. These nonzero mean values can be used to judge the occurrence of unknown disturbances.

Equation (6.1) is a method to test the occurrence of unknown disturbances using the absolute values of innovation process [14].

$$S=\left(\sum_{i=0}^{N}|r_{ek-i}|\right)/N,\ i=0,1,\cdots,N \tag{6.1}$$

Here, r_{ek} is the innovation process occurred at sampling time k, N is a finite window that accumulates within finite range of innovation absolute values. If the N is too large, r_{ek} does not contribute on S sensitively and the latest information on unknown disturbances is not reflected. While N is too small, the latest information r_{ek} is reflected on S very sensitively and the estimator tends to unstable. Therefore, the designer must determine the size of N with trial and error. Based on the value calculated in Equation (6.1), the presence of unknown disturbances are determined by an algorithm shown in Fig. 6.1.

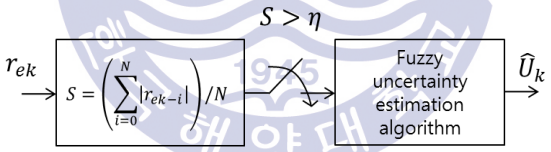

Fig. 6.1 Test for disturbances presence using innovation process

Here, η is a constant defined as the threshold, and η is design value based on the S value. If $S>\eta$ condition is satisfied, it is assumed that an unknown disturbances are applied to the ship, and the estimation value $\widehat{U_k}$ of the unknown disturbances are estimated by the fuzzy disturbance estimation algorithm.

6.2 Fuzzy disturbance estimation algorithm

The existence of unknown disturbances are determined by the method

explained at 6.1 whenever unknown disturbances are applied to the ship. This section explains the comprising method of fuzzy disturbance estimation algorithm to estimate the unknown disturbances. The fuzzy disturbance estimation algorithm is shown in Fig. 6.1 and the variables used are defined in Equation 6.2 [15].

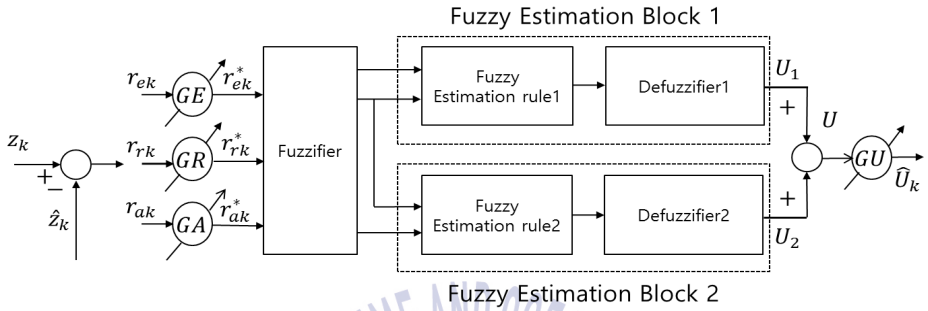

Fig. 6.2 Functional diagram of a fuzzy disturbance estimation algorithm

$$
\begin{aligned}
r_{ek} &= z_k - \hat{z_k} & r^*_{ek} &= GE \times r_{ek} \\
r_{rk} &= r_{ek}/T & r^*_{rk} &= GR \times r_{rk} \\
r_{ak} &= [r_{ek} - r_{ek-1}]/T & r^*_{ak} &= GA \times r_{ak} \\
GE &= L/|r_{ek}| & GR &= L/|r_{rk}| \\
GA &= L/|r_{ak}| & GU &= L/GR \\
U &= U_1 + U_2 & \hat{U}_k &= U \times GU
\end{aligned}
\tag{6.2}
$$

Here, T is a sampling time, r_{rk} is the value of innovation process divided by time T. r_{ak} is the change rate of r_{rk}. GE, GR and GA are the input scale parameters to normalize the values of r_{ek}, r_{rk} and r_{ak}, GU is the scale parameter for defuzzified output U. L is a normalization parameter that normalizes the input and output fuzzy set, and L is determined by the designer. The next thing is how to fuzzify r^*_{ek}, r^*_{rk} and r^*_{ak} into fuzzy sets for

the inputs of fuzzy disturbance estimation algorithm. U_1, U_2 are generated through the fuzzy estimation rule and the defuzzification process. A detailed description of the fuzzification, defuzzification method and fuzzy estimation rule will be described followings.

6.2.1 Fuzzfication algorithm

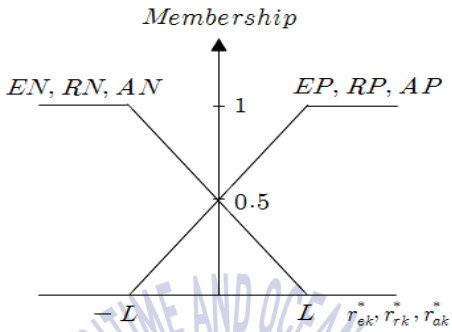

Fig. 6.3 Input fuzzifications for the fuzzy disturbance estimation algorithm

Fig. 6.3 shows fuzzification algorithms of r^*_{ek}, r^*_{rk} and r^*_{ak} mapping into fuzzy sets. r^*_{ek} is mapped into two fuzzy sets of EP and EN. r^*_{rk} is mapped into two fuzzy sets of RP and RN. And r^*_{ak} is mapped into two fuzzy sets of AP and AN.

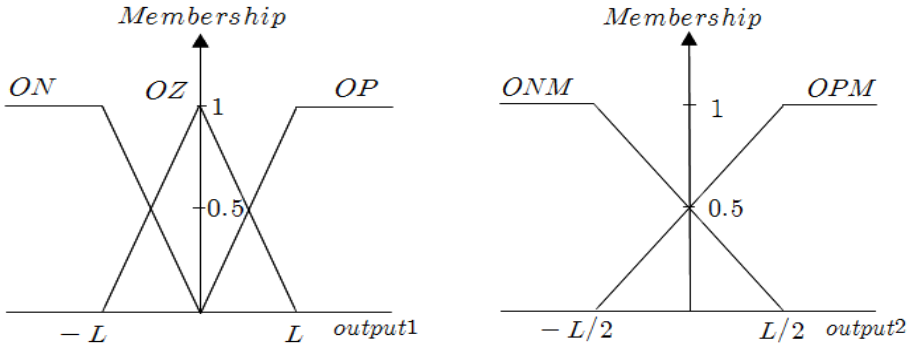

Fig. 6.4 Output fuzzification for fuzzy estimation block 1 and 2

The fuzzy output for U_1 is shown in the left figure of Fig. 3.3, and has three fuzzy sets as OP, OZ and ON. The fuzzy output for U_2 is shown in the right figure of Fig. 6.4, and has two fuzzy sets as OPM and ONM.

6.2.2 Fuzzy estimation rule

Fuzzy estimation rules are created in the form of conditional statements and the estimation rules for fuzzy estimation blocks 1 and 2 are as follows [15].

Fuzzy estimation block 1
$(R1)_1 : IF\ r_{ek}^* = EP$ and $r_{rk}^* = RP\ \ THEN\ \ dU_1 = OP$
$(R2)_1 : IF\ r_{ek}^* = EP$ and $r_{rk}^* = RN\ \ THEN\ \ dU_1 = OZ$
$(R3)_1 : IF\ r_{ek}^* = EN$ and $r_{rk}^* = RP\ \ THEN\ \ dU_1 = OZ$
$(R4)_1 : IF\ r_{ek}^* = EN$ and $r_{rk}^* = RN\ \ THEN\ \ dU_1 = ON$
Fuzzy estimation block 2
$(R1)_2 : IF\ r_{rk}^* = RP$ and $r_{ak}^* = AP\ THEN\ \ dU_2 = OPM$
$(R2)_2 : IF\ r_{rk}^* = RP$ and $r_{ak}^* = AN\ THEN\ \ dU_2 = ONM$
$(R3)_2 : IF\ r_{rk}^* = RN$ and $r_{ak}^* = AP\ THEN\ \ dU_2 = OPM$
$(R4)_2 : IF\ r_{rk}^* = RN$ and $r_{ak}^* = AN\ THEN\ \ dU_2 = ONM$

The estimation rules of fuzzy estimation blocks 1 and 2 are applied with the AND logic of Zadeh for the premise parts, which performs a min operation to find the fitness of the consequent parts of the control rules. The input space is always present within the normalization parameter range $[-L, L]$ according to the magnitude of the input. In order to this, the scale parameter is varied at every sampling time as in Equation (6.3)

$$GE = L/|r_{ek}|\ ,\ GR = L/|r_{rk}|\ ,\ GA = L/|r_{ak}| \tag{6.3}$$

GE, GR, GA and GU, the input spaces for fuzzy estimation blocks 1 and 2 are divided into $(IC1)_1 \sim (IC8)_1$ and $(IC1)_2 \sim (IC8)_2$ respectively in the

interval $[-L, L]$ as shown in Fig. 6.5 and Fig. 6.6.

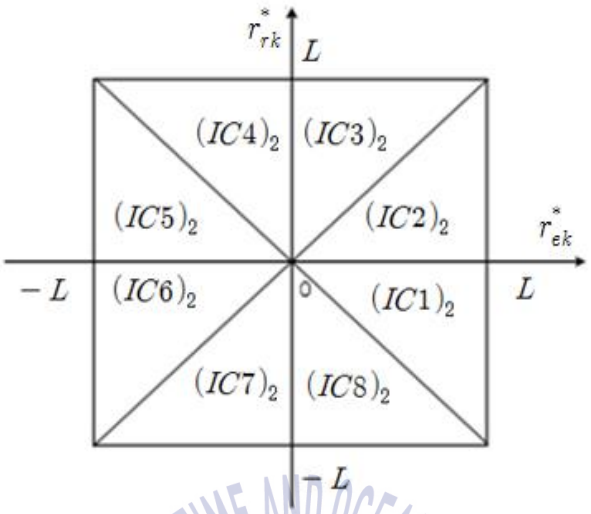

Fig. 6.5 Possible input partitioning for r^*_{ek} and r^*_{rk}

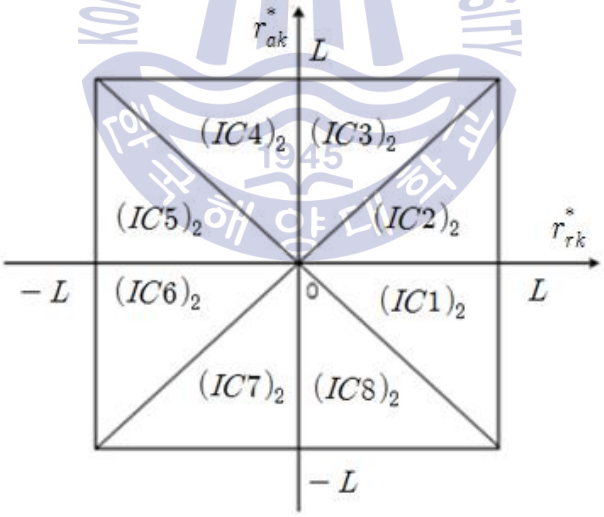

Fig. 6.6 Possible Input partitioning for r^*_{rk} and r^*_{ak}

The defuzzifier algorithm used in the fuzzy disturbance estimation algorithm is weighted center method and the defuzzify output is expressed as Equation (6.4).

$$U = \frac{\sum(membership\ of\ member) \times (value\ of\ member)}{\sum(memberships)} \tag{6.4}$$

Through the defuzzification, Add outputs dU_1 and dU_2 of the fuzzy estimation blocks 1 and 2, and multiplying the output scale parameter GU produces an unknown disturbances estimation value $\widehat{U}_k$ as the final output. $\widehat{U}_k$ is expressed Equation (6.5) ~ Equation (6.8) according to the condition.

$$IF\ GR \times |r_{rk}| \le GE \times |r_{ek}| \le L \text{ and } GA \times |r_{ak}| \le GR \times |r_{rk}| \le L,$$

$$THEN$$

$$\widehat{U}_k = \frac{0.5 \times L \times GU \times GE}{2L - GE \times |r_{ek}|} r_{ek} + \frac{0.5 \times L \times GU \times GR}{2L - GE \times |r_{ek}|} r_{rk}$$

$$+ \frac{0.25 \times L \times GU \times GA}{2L - GR \times |r_{rk}|} r_{ak} \tag{6.5}$$

$$IF\ GR \times |r_{rk}| \le GE \times |r_{ek}| \le L \text{ and } GR \times |r_{rk}| \le GA \times |r_{ak}| \le L,$$

$$THEN$$

$$\widehat{U}_k = \frac{0.5 \times L \times GU \times GE}{2L - GE \times |r_{ek}|} r_{ek} + \frac{0.5 \times L \times GU \times GR}{2L - GE \times |r_{rk}|} r_{rk}$$

$$+ \frac{0.25 \times L \times GU \times GA}{2L - GA \times |r_{ak}|} r_{ak} \tag{6.6}$$

$$IF\ GR \times |r_{ek}| \le GE \times |r_{rk}| \le L \text{ and } GA \times |r_{ak}| \le GR \times |r_{rk}| \le L,$$

$$THEN$$

$$\widehat{U}_k = \frac{0.5 \times L \times GU \times GE}{2L - GR \times |r_{rk}|} r_{ek} + \frac{0.5 \times L \times GU \times GR}{2L - GR \times |r_{rk}|} r_{rk}$$

$$+ \frac{0.25 \times L \times GU \times GA}{2L - GR \times |r_{rk}|} r_{ak} \tag{6.7}$$

$$IF\ GE\times\left|r_{ek}\right| \le GR\times\left|r_{rk}\right| \le L \text{ and } GR\times\left|r_{rk}\right| \le GA\times\left|r_{ak}\right| \le L,$$

$$THEN$$

$$\hat{U}_k = \frac{0.5\times L\times GU\times GE}{2L-GR\times\left|r_{rk}\right|}r_{ek} + \frac{0.5\times L\times GU\times GR}{2L-GR\times\left|r_{rk}\right|}r_{rk}$$

$$+ \frac{0.25\times L\times GU\times GA}{2L-GA\times\left|r_{ak}\right|}r_{ak} \tag{6.9}$$

If the scale parameter is changed at every sampling time as in Equation (6.3), the denominators of Equation (6.5) to Equation (6.8) are always L. So unknown disturbance estimation value $\widehat{U}_k$ is given by Equation (6.9).

$$\hat{U}_k = E_i r_k + E_p r_{rk} + E_d r_{ak} \tag{6.9}$$

Here, E_i, E_p, E_d is expressed by Equation (6.10).

$$E_i = 0.5\times GU\times GE,\ E_p = 0.5\times GU\times GR,\ E_d = 0.25\times GU\times GA \tag{6.10}$$

6.2.3 Kalman filter based state estimation algorithm with fuzzy disturbance estimation algorithm

When unknown disturbances are applied, the existence of the unknown disturbances are determined based on the innovation process of the Kalma filter. If the existence is judged, the unknown disturbance estimation value $\widehat{U}_k$ is estimated as Equation (6.9) through the fuzzy disturbance estimator. At this time, if the estimated value $\widehat{U}_k$ is feedback to the Kalman filter algorithm at the next sampling time, a state estimation algorithm capable of estimating an actual state can be constructed. This can be expressed as Equation (6.11).

$$
\begin{aligned}
&\hat{x}_k(-) = A\hat{x}_{k-1} + Bu_{k-1} + \hat{U}_{k-1} \\
&P_k(-) = AP_{k-1}(+)A^T + Q \\
&K_k = P_k(-)C^T\left[CP_k(-)C^T + R_k\right]^{-1} \\
&\hat{x}_k = \hat{x}_k(-) + K_k\left[z_k - C\hat{x}_k(-)\right] \\
&P_k = \left[I - K_kC\right]P_k(-) \\
&\hat{U}_k = E_i r_{ek} + E_p r_{rk} + E_d r_{ak}
\end{aligned}
\tag{6.11}
$$

Here, the unknown disturbance estimation value $\hat{U}_k$ is feedback to calculate a predicted value of the next sampling time. $\hat{U}_k$ is calculated only when Equation (6.1) is satisfied, If otherwise, the previous value is used continuously.

6.3 Proposal of fuzzy PID autopilot system based on Kalman filter with unknown disturbance estimator

When the unknown disturbances estimator is used for Kalman filter based state estimation algorithm, and fuzzy PID autopilot system based on Kalman filter comprises using separation principle. Fig. 6.7 is block diagram of a fuzzy PID type autopilot system that estimates the magnitude of unknown disturbances by the fuzzy disturbance estimator when unknown disturbances are applied. The estimated disturbances magnitude $\hat{U}_k$ is feedback to Kalman filter to compensate filter update and also feedback to the output side of fuzzy PID autopilot to compensate the control performance degraded by unknown disturbances.

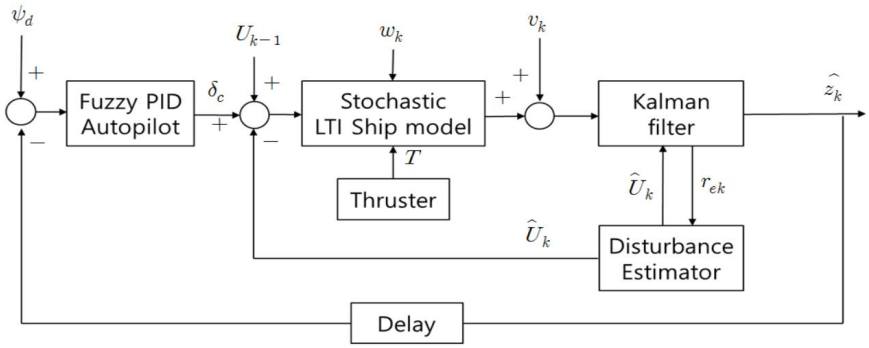

Fig. 6.7 Block diagram of fuzzy PID autopilot system based on Kalman filter with fuzzy disturbance estimator

The ship model used in the simulation is the same condition as section 5.4. The purpose of simulation is whether the fuzzy disturbance estimator estimates unknown disturbances well or not and to verify the performance of ship motion when $\hat{U}_k$ is feedback.

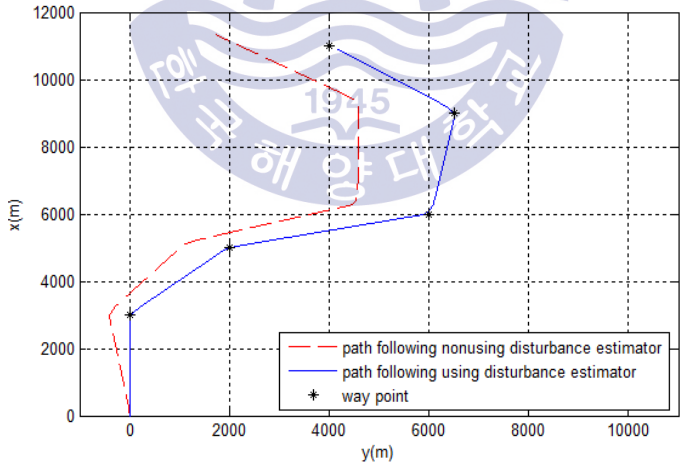

Fig. 6.8 Comparison of path following with and without disturbance estimator

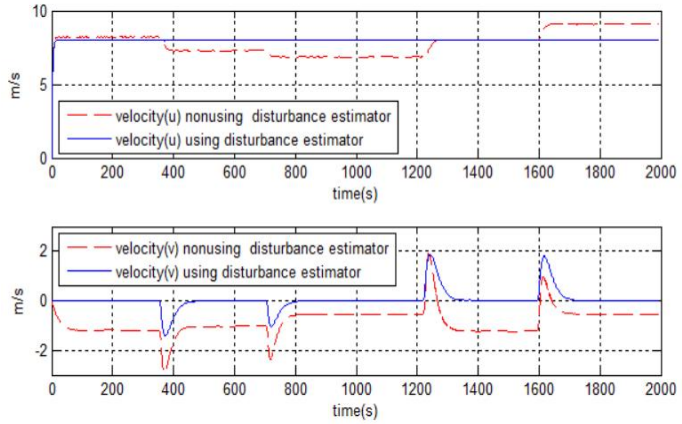

Fig. 6.9 Comparison of ship speed with and without disturbance estimator

Fig. 6.8 shows the simulation result of the comparison of path following with and without disturbance estimator. If unknown disturbances are applied, the ship can not maintain the designated route. But if the forces and moments added to the ship due to unknown disturbances are estimated and feedback the ship moves with nearly small deviation from the designated route. Fig. 6.9 shows the simulation result of the comparison of ship speeds with and without disturbance estimator. When unknown disturbances are applied, the ship cannot maintain the initial set value $8m/s$ in the forward direction speed, and also the lateral speed is occurred even in the range except the course change. For this reason, the ship deviates from the designated route. However, If the forces and moments added to the ship are estimated and feedback, it can be seen that the ship maintain the initial set value $8m/s$ in the forward direction speed and the lateral speed also is not occurred in the section except the course change. The reason why the ship can operate without deviating the route is that the fuzzy disturbance estimator normally estimates the forces and moments added to the ship. Fig. 6.10 shows the estimated unknown disturbances.

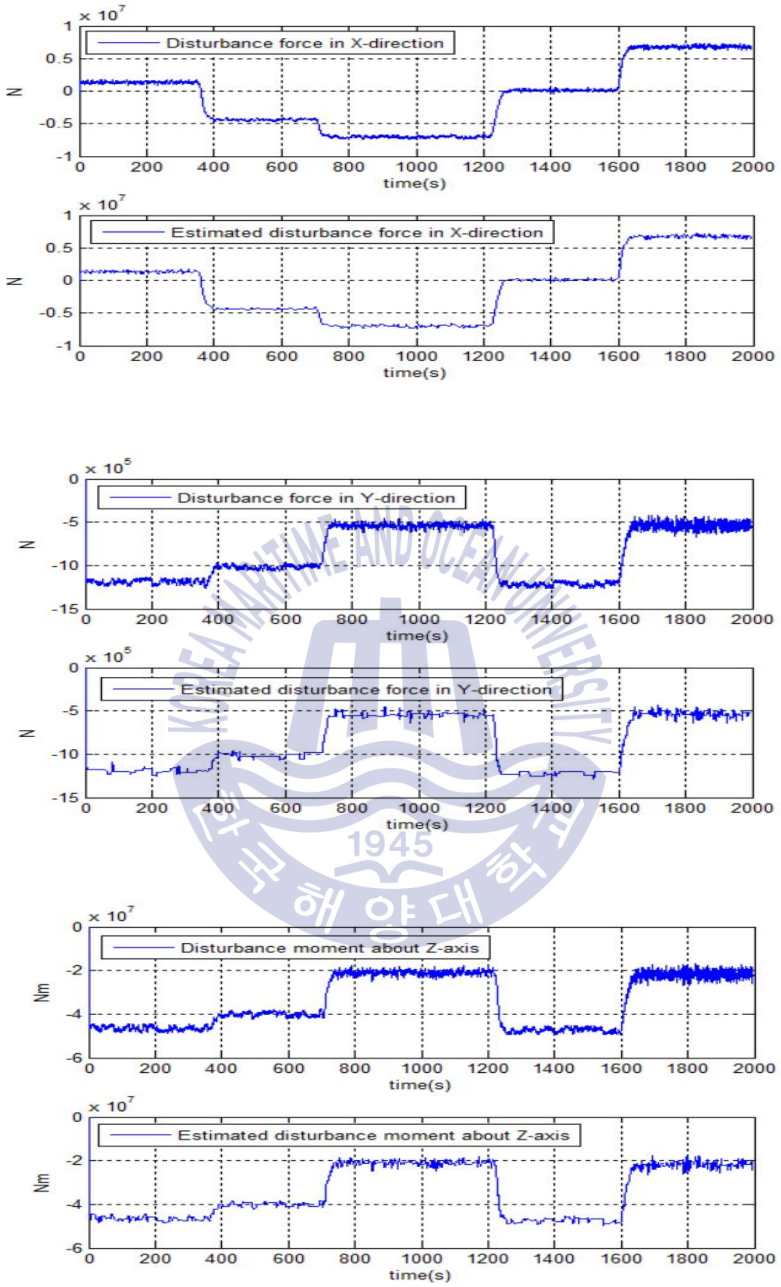

Fig. 6.10 Estimated disturbances by fuzzy disturbance estimator

Fig. 6.10 shows comparison between the forces and moments added to the ship due to unknown disturbances and estimated forces and moments from fuzzy disturbance estimator. It can be seen that the fuzzy disturbance estimator normally estimates the forces and moments added to the ship. Fig 6.11 shows the innovation processes of the Kalman filter with unknown disturbance estimator

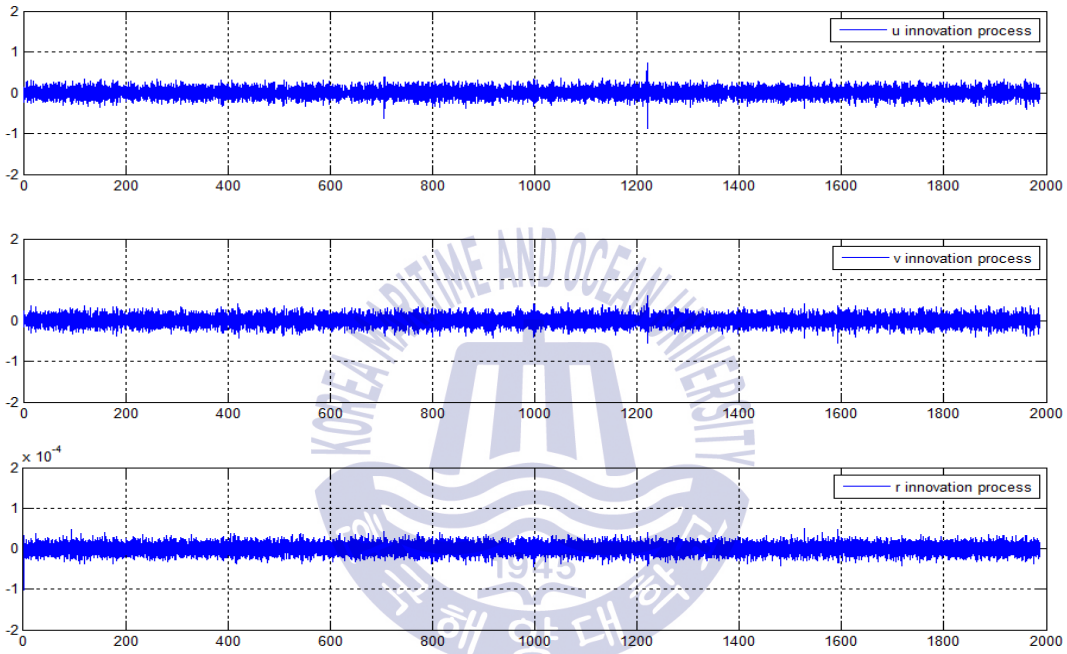

Fig 6.11 Innovation process using disturbance estimator

If the unknown disturbances are applied, the statistical expectation of innovation process does not converge to 0 as shown in Fig. 5.10, so that the state estimation error is constantly generated in the Kalman filter. However if the magnitude of the unknown disturbances are estimated by the fuzzy disturbance estimator and feedback, as shown in Fig 6.11, the statistical expectation of the innovation process converges to 0, which indicates that the Kalman filter correctly estimates the state.

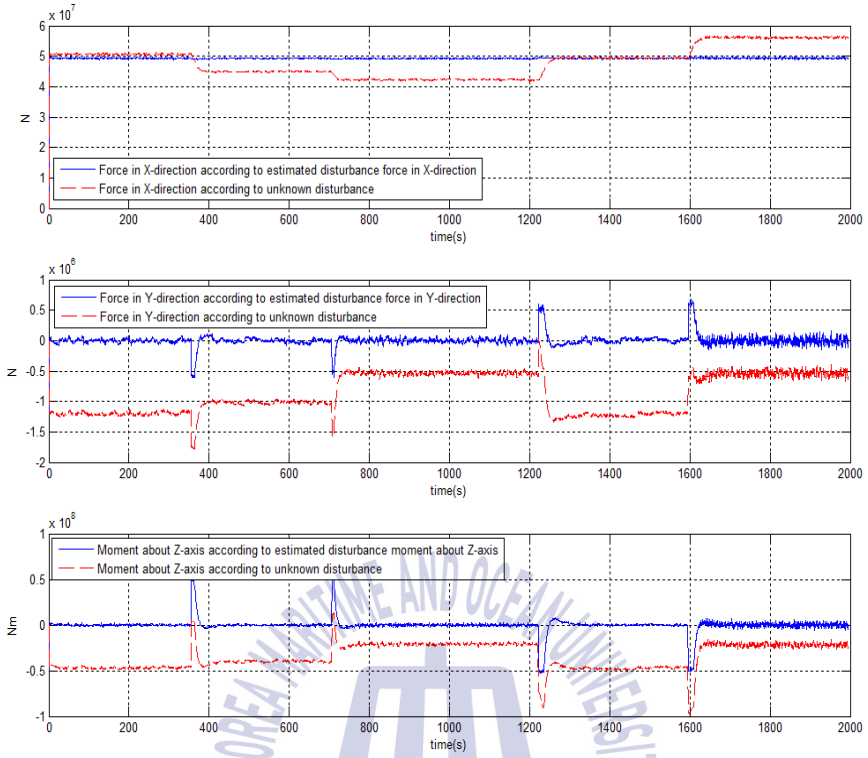

Fig. 6.12 Comparison of forces and moments with and without disturbance estimator

Fig. 6.12 shows simulation results comparing the forces and moments of the ship with and without the fuzzy disturbance estimator when unknown disturbances are applied. If unknown disturbances are applied to the ship, the ship cannot maintain $8m/s$ due to the additional force in the x-direction. However, if the fuzzy disturbance estimator is used to estimate the magnitude of the additional force in the x-direction and feedback estimated force, it can be seen that additional force in the x-direction is reduced. So the ship can move with $8m/s$. If unknown disturbances are applied to the ship, the force in the y-direction and the moment about z-axis are added, so the ship deviates from the designated route. However, if the fuzzy disturbance estimator estimate the force in the y-direction and the moment about z-axis and feedback them, the ship can be operated without deviating from the

designated route because the forces and moments are not generated in the range excluding the course change. In chapter 6, the forces and moment are estimated by using the fuzzy disturbance estimator and feedback to reduce the effect of unknown disturbances. But it is not suitable for the actual situation because it dose not use the propeller and rudder of the ship. Therefore, in chapter 7, we try to convert the estimated unknown disturbances value to the added thrust and rudder angle of the ship. And it is verified that the ship can operate without deviating from the designated route by added thrust and rudder angle.

Chapter 7 Conversion of the estimated value of unknown disturbances to propeller thrust and rudder angle

In chapter 6, Fuzzy disturbance estimator based on Kalman filter innovation process was developed in order to estimate the magnitude of the force and moment added to the ship when the unknown disturbances are applied. And the estimated values were feedback to compensate for the effect of unknown disturbances. However, it is not possible for actual problem to reduce the influence of unknown disturbances by simply feedback, because ship has only two actuators such as propeller and rudder, and there are no instruments to directly realize the feedback mechanism for the estimated values. Therefore, in order to implement the feedback problem, chapter 7 attempts to convert the estimated unknown disturbance values into the propeller thrust and rudder angle of ship.

$$\begin{bmatrix}\dot{u}\\ \dot{v}\\ \dot{r}\end{bmatrix}=\begin{bmatrix}c & 0 & 0\\ 0 & a_{11} & a_{12}\\ 0 & a_{21} & a_{22}\end{bmatrix}\begin{bmatrix}u\\ v\\ r\end{bmatrix}+\begin{bmatrix}b & 0\\ 0 & d_1\\ 0 & d_2\end{bmatrix}\begin{bmatrix}T\\ \delta\end{bmatrix}+\begin{bmatrix}-c\cos(\beta-\psi-\psi_H)V_c+X_{wind}\\ -a_{11}\sin(\beta-\psi-\psi_H)V_c+Y_{wind}\\ -a_{21}\sin(\beta-\psi-\psi_H)V_c+N_{wind}\end{bmatrix} \tag{7.1}$$

Equation (7.1) is the state space equation of the ship when unknown disturbances are applied. The last term of the right-hand side of Equation (7.1) represents unknown disturbance mathematical models which are actually

unmodelled in real situation. In control problem, the unknown term can be substituted by the estimated disturbances, as shown in Equation (7.2) For convenience, the estimated values of the unknown disturbances in the x,y -direction and z-axis are defined as $\widehat{U}_k(x)$, $\widehat{U}_k(y)$ and $\widehat{U}_k(z)$.

$$\begin{bmatrix}\dot{u}\\ \dot{v}\\ \dot{r}\end{bmatrix}=\begin{bmatrix}c & 0 & 0\\ 0 & a_{11} & a_{12}\\ 0 & a_{21} & a_{22}\end{bmatrix}\begin{bmatrix}u\\ v\\ r\end{bmatrix}+\begin{bmatrix}b & 0\\ 0 & d_1\\ 0 & d_2\end{bmatrix}\begin{bmatrix}T\\ \delta\end{bmatrix}+\begin{bmatrix}\widehat{U}_k(x)\\ \widehat{U}_k(y)\\ \widehat{U}_k(z)\end{bmatrix} \tag{7.2}$$

If the estimated values of unknown disturbances are used as Equation (7.2), it is possible to convert the estimated values into the propeller thrust and rudder angle of ship.

Since the propeller thrust T affects only $\dot{u}$, it is possible to define the propeller thrust added to the ship as $T(x)$ that makes $\widehat{U}_k(x)$ to 0. By the way, since there is only one rudder on the ship for steering control, it is impossible to find the rudder angle that make $\widehat{U}_k(y)$ and $\widehat{U}_k(z)$ to 0 at the same time. So, in this paper, the rudder angle added to the ship is made in the manner that the average of $\widehat{U}_k(y)$ and $\widehat{U}_k(z)$ is going th be zero. At this time, the rudder angle added to the ship is defined as $\delta(yz)$.

$$\begin{bmatrix}\dot{u}\\ \dot{v}\\ \dot{r}\end{bmatrix}=\begin{bmatrix}c & 0 & 0\\ 0 & a_{11} & a_{12}\\ 0 & a_{21} & a_{22}\end{bmatrix}\begin{bmatrix}u\\ v\\ r\end{bmatrix}+\begin{bmatrix}b & 0\\ 0 & d_1\\ 0 & d_2\end{bmatrix}\begin{bmatrix}T+T(x)\\ \delta+\delta(yz)\end{bmatrix} \tag{7.3}$$

Equation (7.3) is the state space equation of the ship, which has the added propeller thrust and added rudder angle as a method to compensate or to feedback the estimated unknown disturbance values.

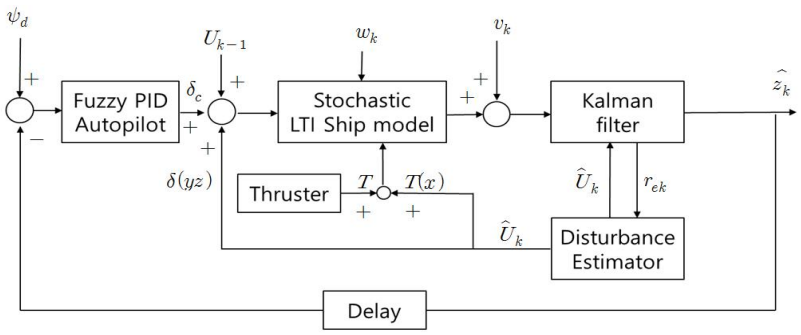

Fig. 7.1 Block diagram of fuzzy PID autopilot system, which converts the $\hat{U}_k$ into the thrust and steering angle added to the ship

The ship model used in the simulation is the same that used in section 5.4. Only the difference is that the estimated values of unknown disturbances are converted to the thrust $T(x)$ and rudder angle $\delta(yz)$ added to the ship. In order to verify the control performance of the autopilot system suggested in Fig. 7.1, simulations are performed and the effectiveness of the suggested control system is assured by analyzing simulation results.

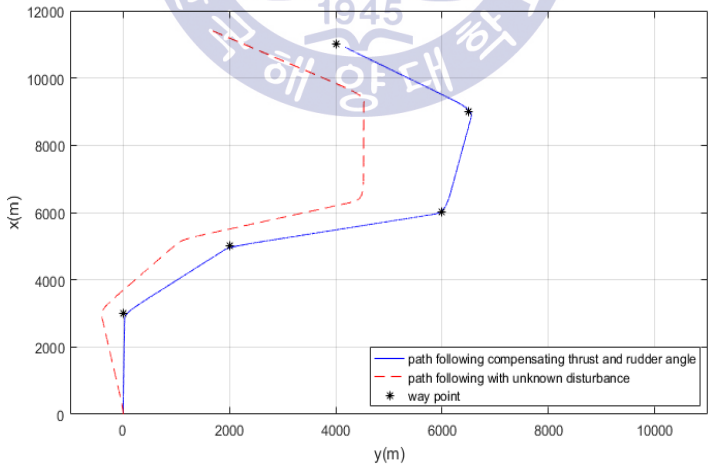

Fig. 7.2 Path following comparison between with and without the compensated rudder angle and thrust

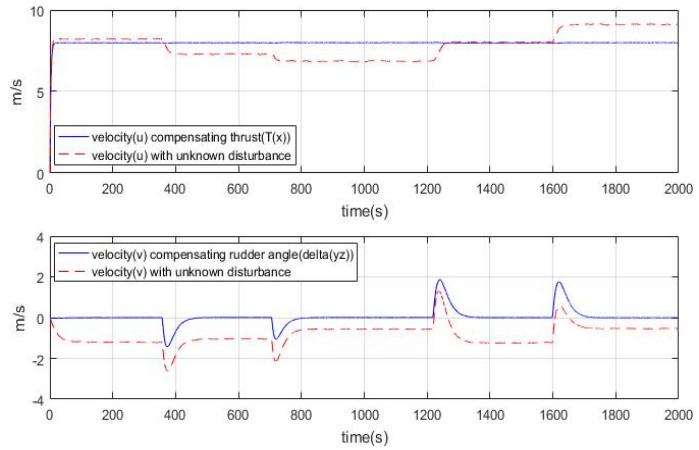

Fig. 7.3 Velocity comparison between with and without the compensated rudder angle and thrust

Fig. 7.2 shows the simulation result of movement of the ship by compensating the added thrust $T(x)$ and added rudder angle $\delta(yz)$. The ship cannot follow the designated route just like the result of simulation by feedback, but the ship can follow the designated route closely. Fig. 7.3 shows simulation result of the velocity of ship by compensating the added thrust $T(x)$ and added rudder angle $\delta(yz)$ using the estimated value of the unknown disturbances. It can be also seen that the initial velocity set value $8m/s$ in the forward direction is maintained and the lateral velocity component does not occur in the range excluding the alter course.

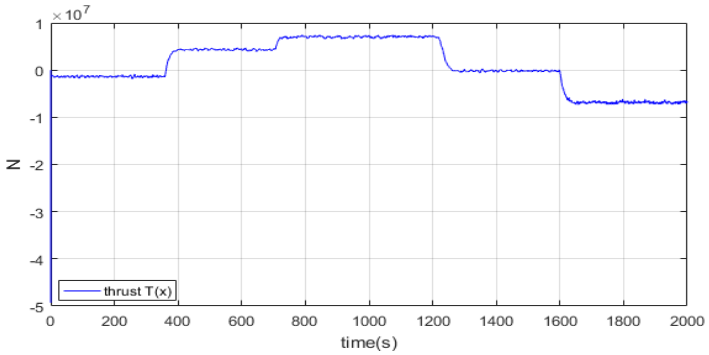

Fig. 7.4 The compensated thrust $T(x)$

The forward speed of the ship cannot be maintained at the initial set value $8m/s$ due to influence of the unknown disturbances. Therefore, it is necessary to compensate the propeller thrust. Fig. 7.4 is a simulation result showing the thrust added to the ship to reduce the influence of the unknown disturbances.

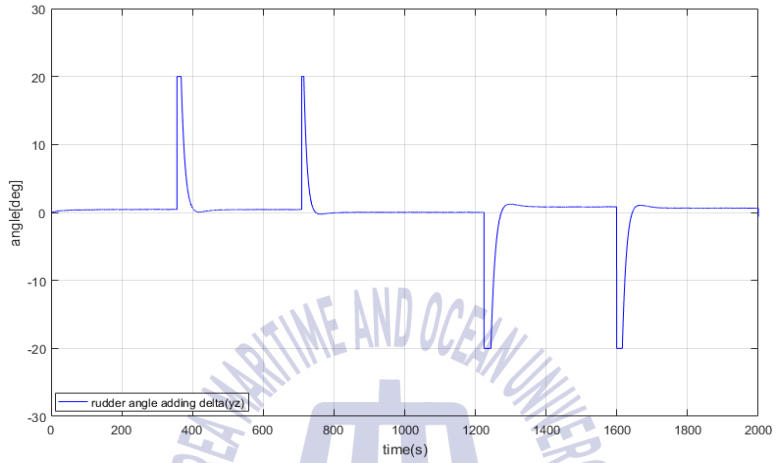

Fig. 7.5 Total rudder angle added the compensated $\delta(yz)$

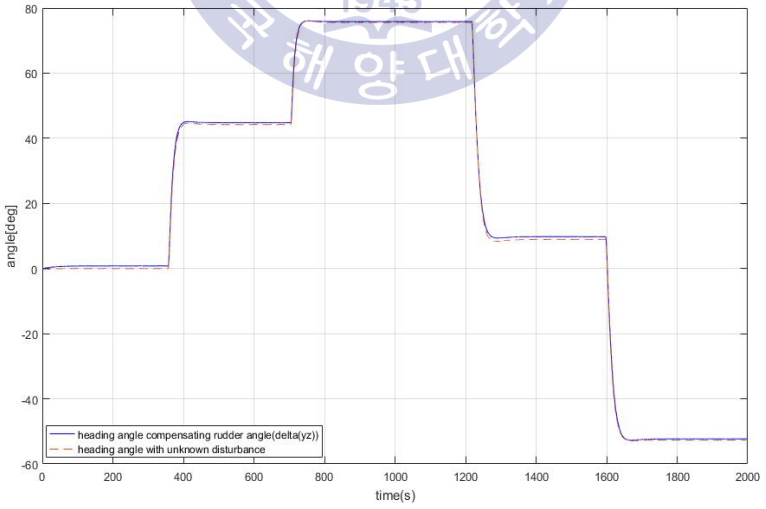

Fig. 7.6 Heading angle comparison between with and without the compensated rudder angle $\delta(yz)$

If the unknown disturbances are applied, the ship moves maintaining the heading angle due to autopilot system, but deviates from the designated route because the additional forces and moment are applied to the ship. In order to solve this problem, chapter 7 attempted to compensate the propeller thrust and rudder angle of ship with the $T(x)$ and $\delta(yz)$. Fig. 7.5 shows the simulation result of the total rudder angle in case the rudder angle $\delta(yz)$ is compensated by the estimated value of unknown disturbances. It can be seen that the ship has the total rudder angle resulted from the autopilot rudder angle δ_c plus the additional rudder angle $\delta(yz)$ to reduce the effects of the unknown disturbances. As shown in Fig. 7.6, it can be seen that the ship does not operate maintaining the reference heading angle. However the purpose of this paper is to operate the ship without deviating from the designated route. In order to satisfy the route tracking purpose, the ship can not shep taking the heading angle slightly different from the reference heading angle.

Chapter 8 Conclusion

In this paper, a velocity type fuzzy PID autopilot system was suggested to compensate for the disadvantages of the PD type autopilot system. And also, a method to combine the velocity type autopilot with state estimation algorithm based on Kalman filter by using the separation principle, was suggested. Using the separation principle, the control performance is improved when the noises are included. In addition, based on the innovation characteristics of the Kalman filter, a fuzzy disturbance estimation algorithm was developed to estimate the unknown disturbances. By estimating the magnitudes of the unknown disturbances by the fuzzy estimation estimator and feeding back them, the ship could stably follow the designated route despite that the unknown disturbances were applied to the ship. In the conclusion, the velocity type fuzzy PID autopilot system based on Kalman filter with disturbance estimator was suggested, the control performance of it was verified. The procedure to develop the suggest autopilot system in this paper is summarized as follows.

(1) The PD type autopilot system, which has been widely used as the heading angle keeping controller, occurs the overshoot due to the rough rudder angle change in case that the rudder command angle is large. This

reason causes the energy loss of ship under navigation. But if the velocity type fuzzy PID autopilot system is used, overshoot is rarely occurred even if the rudder angle change is large, and time required to reach the reference heading angle is relatively fast compared with the PD controller. Also simulation results show that rudder angle change is smooth and the energy loss of the ship can be reduced.

(2) The velocity type fuzzy PID autopilot system under noises has poor control performance in steady state due to malfunction of D control. In order to improve the steady state performance under noises, the Kalman filter was adopted to estimate the noisy output. Therefore, the velocity type fuzzy PID autopilot system based on Kalman filter was suggested using separation principle. Through simulations, it was verified that the steady state performance of the suggested autopilot system was improved even under noises.

(3) Even though velocity type fuzzy PID type autopilot with excellent performance is applied, if the unknown disturbances such as current, wave, and wind are applied to the ship, not only the ship cannot maintain the initial set speed in the forward direction and but also speed in the lateral direction is occurred even during no course change. As a result, the forces and moment by unknown disturbances are added to the ship, and the ship cannot maintain the designated route. In order to solve this problem, the fuzzy disturbance estimator using Kalman filter innovation characteristics was designed. Through simulations, it was found that fuzzy disturbance estimator estimated the unknown disturbances approximately.

(4) The estimated unknown disturbances were feedback to compensate Kalman filter so that the Kalman filter can normally estimate the state even if unknown disturbances were applied. Simulation results proved that the expected value of the Kalman filter innovation process converged to zero in

steady state. And also, the estimated unknown disturbances were feedback to the output part fuzzy PID controller to generate the resultant control input. Therefore, the final structure of the suggested autopilot system was completed, named the velocity type fuzzy PID autopilot system based on Kalman filter with disturbance estimator.

(5) In order to apply the suggested autopilot system to real autopilot system, the estimated disturbances must be allocated to propeller and rudder. For this work, the conversion algorithm was suggested, which converted the estimated disturbances to additional propeller thrust and additional rudder angle. Through simulations, it was proven that the ship could follow the designated route with good performance in spite of unknown disturbances.

Reference

[1] E. Sperry, "Directional Stability of Automatically Steered Bodies" Journal of the American Society of Naval Engineering, Vol. 42, NO. 2, 1992.

[2] T. I. Fossen, "Recent Development in Ship Control Systems Deign," World super-yacht Review, Sterling Publication Limited, 1999.

[3] T. I. Fossen, Handbook of Marine Craft Hydrodynamics and Motion Control, Sussex, England: John Willy & Sons Ltd, 2011.

[4] O. M. Faltinsen, Sea Loads on Ship and Offshore Structures, New York, USA: Cambridge University Press, 1990.

[5] T. I. Fossen, Guidance and Control of Ocean Vehicles, Sussex, England: John Willy & Sons Ltd, 2011.

[6] R. Satun and G. N. Roberts, "Approaches to Fuzzy Autopilot Design Optimization," Proceedings of the 4th IFAC conference on Maneuvering and Control of Marine Craft, pp. 77-82, 1997.

[7] B. K. Lee, J. H. Hwa, "Yaw Angle Command Generation and Adaptive Fuzzy control for Automatic Route Tracking of Ships," The Korean Society of Marine Engineering, Vol. 25, No. 1, pp. 199-208, 2001.

[8] G. E. Hearn, Y. Zhang and P. Sen, "Alternative Designs of Neural Network Based Autopilots : A Comparative study," Proceedings of the 4th IFAC conference on Maneuvering and Control of Marine Craft, pp. 83-88, 1997.

[9] K. E. Husa and T. I. Fossen, "Backstepping Designs for Nonlinear Way-Point Tracking" of the 4th IFAC conference on Maneuvering and Control of Marine Craft, 1997.

[10] B. K. Lee, J. H. Hwa, "A Study on the Automatic Route Tracking Control of a Ship Using an Adaptive Fuzzy Controller," Proceedings of the 14th Korea Automatic Control Conference, 1999.

[11] I. H. Kim, "A Study on the Design Method of a Nonlinear Fuzzy PID Controller with Variable Parameters," Department of Control & Instrumentation Engineering, Graduate School, Korea Maritime University, Doctoral dissertation, 2004.

[12] B. K. Lee, "An Optimal Route Decision and LOS Guidance system for Automatic Navigation of Ships," Department of Control & Instrumentation Engineering, Graduate School, Korea Maritime University, Doctoral dissertation, 2005.

[13] B. H. Choi, "A Study on the Integrated Control of Ship Motion Based on Joystick Control," Department of Control & Instrumentation Engineering, Graduate School, Korea Maritime University, Master's dissertation, 2011.

[14] S. K. Seo "State Estimation Algorithm with Fuzzy Estimation Technique for Linear Time Invariant Uncertain System," Department of Control & Instrumentation Engineering, Graduate School, Korea Maritime University, Master's dissertation, 2013.

[15] S. H. Park, "State Estimation and Control of Stochastic System under Unknown disturbances and Noise," Department of Control & Instrumentation Engineering, Graduate School, Korea Maritime University, Master's dissertation, 2016.

[16] B. K. Lee "A Study on the Automatic Route Tracking Algorithm of Ships," Department of Control & Instrumentation Engineering, Graduate School, Korea Maritime University, Master's dissertation, 1999.

[17] J. H. Kim, Y. S. Ha, B. K. Lee, "A Fuzzy PID Controller Type Autopilot System for Route-Tracking of Ships," The Korean Society of Marine Engineering, Vol. 30, No. 6, pp. 760-769, 2006.

[18] R. M. Isherwood, "Wind Resistance of Merchant Ships," Jonrnal of the Royal Institution Naval Architects," Vol. 115, pp. 327-338, 1972.